POLITECNICO DI TORINO

Faculty of Aerospace Engineering

Master Thesis

# Design and Validation of a Flexible Spacecraft Model for Attitude Control Applications

**Supervisor:**
Dr. Elisa Capello

**Co-supervisors:**
Dr. Mauro Mancini
Ing. Daniele Catelani

**Candidate:**
Gianluca Tagliani

July 2022

*To my family and whoever supported me during this university experience.*

# Acknowledgements

I would like to thank my supervisors Dr. Elisa Capello and Dr. Mauro Mancini for their help and constant presence during the whole period of the thesis. Last but not least, a heartfelt thank you also to Ing. Daniele Catelani for his availability and patience shown me during the intensive learning of the software MSC Adams.

# Abstract

The purpose of this thesis is the assessment of a comparison between a flexible spacecraft model, studied during previous theses and scientific articles, and the implementation of the same spacecraft in the software MSC Adams, aiming at validating the model. Thanks to this innovative tool it is possible to evaluate several features the user could desire to have available, conducting a non-linear multi-body analysis, that allows to provide more realistic data sets.
The Picard satellite of the French Space Agency (CNES) is used as the main body of the spacecraft and its dynamics is expressed with Euler equations for a rigid body. The configuration, in terms of locations and dimensions, of the solar panels and the reaction wheels has been modified with respect to Picard in order to have advantages during the construction of the spacecraft in MSC Adams and to have a more general type of satellite. In particular, four symmetrical solar panels and a system of three reaction wheels located at the center of mass of the spacecraft are considered. The most important aspect of the work is the flexible part of the satellite, represented by the four solar panels. A Finite Element Method (FEM) analysis with MSC Patran/MSC Nastran is conducted to obtain the natural modes and frequencies necessary for the model and a coupling matrix between rigid and flexible part is also evaluated.
The second part of the thesis is about the spacecraft design implementation in MSC Adams View and the simulation phases, which are made through both MSC Adams and MATLAB/Simulink environment. A simple Proportional-Derivative (PD) controller is implemented for the attitude control during a manoeuvre, with the purpose of achieving the desired Euler angles, aiming at simulating a command for a new pointing direction towards a particular objective. The comparison between the two models is done in order to understand better the influence of the flexibility of the solar panels and the possible differences between the more complex analysis in MSC Adams and the linearized, more approximated one through the mathematical model. The attitude control in case of failure of three solar panels is also assessed. The PD controller ensures good performance and a stable response during the manoeuvre, despite of the external (only the gravity gradient is taken into consideration) and internal (vibrations of the solar panels) disturbances acting on the system. Nevertheless, this basic controller has some problems in case of failure of the panels.

# Contents

# List of Figures

# List of Tables

# Chapter 1

# Introduction

In control applications, spacecraft are often modelled as a rigid body, which is acceptable if the satellite has no large moving parts and its structure is mainly composed of a single body. However, satellites often have moving parts such as large flexible solar panels, robotic arms, telescopic booms, tethers or liquid fuel. In this case, the dynamic coupling effects between the moving parts are not negligible, and in order to take into account their effects on the overall system dynamics, the rigid-body model must be dismissed. Indeed, in a multi-body satellite the movement of one of the bodies disturbs position and attitude of the whole space robot. This is due to internal forces and torques exchanged between the bodies at their connection points, i.e. the joints. In addition, the coupling between the flexibility of the structure and the attitude dynamics causes vibrations of the flexible bodies and internal torques acting on the satellite and disturbing the attitude dynamics [1].

## 1.1 Goals of the work

The scope of this thesis is the development of two models to simulate the attitude dynamics of a flexible spacecraft. The first one is based on a mathematical model already present in literature [2], the second one is implemented through the software MSC Adams. Accurate models of satellite attitude dynamics are of fundamental importance for Guidance, Navigation and Control (GNC) systems. In general, a GNC system consists of three main parts:

- Guidance: provides at each point the reference values for the state vector in time, that is then compared with the estimated actual values, provided by the navigation function.
- Navigation: consists of a Kalman filter, which provides the controller and the guidance functions with the necessary information on the actual state of the spacecraft.

- Control: provides the force and torque commands necessary to achieve the desired corrections in attitude and trajectory.

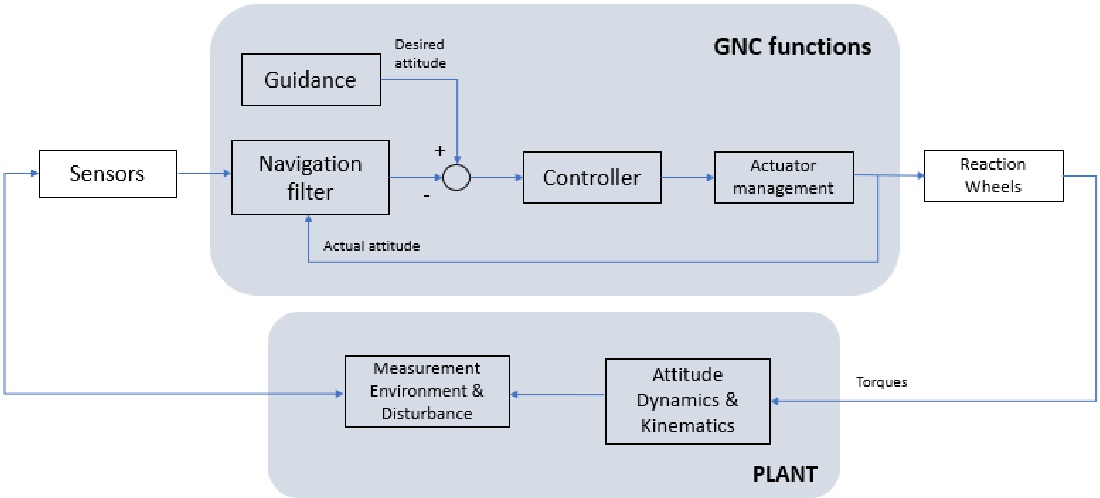


Figure 1.1: Attitude GNC system [3].

The GNC system includes both the components used for position dynamics and the components used by the Attitude Determination and Control System (ADCS). The ADCS part includes all the sensors for the attitude determination, such as star trackers, sun sensors, horizon sensors, magnetometers, and gyros. The controller computes the torque required to steer the attitude error to zero. This torque is the input of the actuator system, that can include thrusters, reaction wheels, control moment gyros and magnetorquers. In this work, the navigation system is not studied, and the actual state informations are given by the plant of the system, defined by the attitude kinematics and dynamics. Moreover, the actuator system is represented by the reaction wheels, and the control function is based on a PD controller. [3] Since the primary goal was to validate the flexible spacecraft mathematical model, the same attitude controller has been implemented on both the two models. To make it simpler a basic PD regulator has been chosen, conscious that it is not the most efficient controller to obtain high attitude performance.

## 1.2 Picard spacecraft

Picard (Fig. 1.2) is a CNES solar-terrestrial microsatellite mission of the Myriade series with French multi-institutional and international cooperation. The overall objective is to monitor the solar diameter, the differential rotation, the solar constant (simultaneous measurement of the absolute total and spectral solar irradiance), and to study the long-term nature of their interrelations.

Figure 1.2: Picard satellite [4].

The mission was named in honor of the 17th century French astronomer Jean Picard (1620-1682), who made the first long-term measurements of the solar diameter, observed sunspots, and determined the rotational velocity of the sun. Picard was also the first who accurately measured the length of a degree of a meridian (longitude line) and from that result estimated the size of the Earth. Beyond the determination of the Earth orbit eccentricity, the diameter measurements brought important information about the particular state of the sun during the so-called Maunder Minimum [named after E. W. Maunder (1851-1928), an English astronomer who studied solar records of the period 1645-1715], a period showing a quasi absence of sunspots as compared to the early 17th century. The Maunder Minimum coincided with the middle - and coldest part - of the so-called ‘Little Ice Age’, during which Europe and North America, and perhaps much of the rest of the world, were subjected to bitterly cold winters.

The Picard microsatellite consists of a box-like structure (90 cm x 80 cm x 110 cm) with a single solar panel. The platform structure is made of a massive aluminium base plate, interfacing with the launcher, 4 aluminium strouts supporting the payload plate, and 4 lateral honeycomb panels. An additional carbon carbon plate was added between the payload aluminium deck and the SODISM instrument, to provide a very stable interface and avoid the transmission of any effort to the SODISM mounting points.

The platform is three-axis stabilized. The AOCS (Attitude and Orbit Control Subsystem) is required to provide a pointing accuracy of $< 36$ arcsec for the Z-axis of the S/C, a stability of $< 5$ arcsec/s of the X and Y axis, and 2 arcmin/s about the Z-axis. This level of performance is higher than the performances guaranteed by a standard Myriade platform. Attitude sensing is provided by a star sensor, sun sensors, a magnetometer, and/or by the payload telescope; actuation is provided by a set of reaction wheels, and magnetic rods.

A new sun sensor SES (Senseur d'Ecartométrie Solaire) was developed along with a new fine pointing mode to provide the stringent pointing requirements of Picard. SES is composed of two parts: an optical front part and an electronic back part. The optical part is a narrow bandwidth filter at 782 nm in the solar continuum allowing to be not disturbed by sunspots presence. The filtered Sun image is projected on the four quadrants detector of the electronic back part. Each photodiode of the detector provides a voltage output proportional to the received light intensity. The two parts of the SES are directly mounted on the SODISM instrument to minimize the misalignments [4].

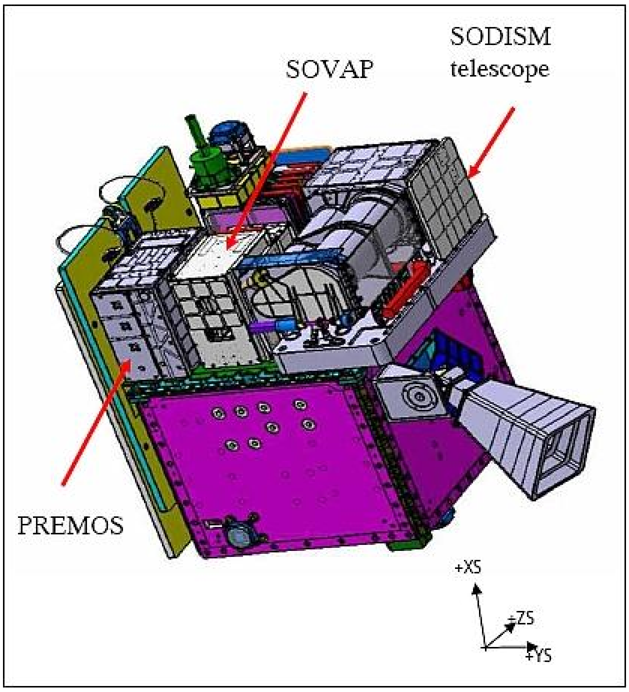


Figure 1.3: PICARD payload [4].

The PICARD payload (Fig. 1.3) is composed of the following instruments:

- SOVAP (SOlar VAriability PICARD): composed of a differential radiometer and a bolometric sensor to measure the total solar irradiance (previously called solar constant);
- PREMOS (PREcision MOnitor Sensor): a set of 3 photometers to study the ozone formation and destruction, and to perform helioseismologic observations, and a differential radiometer to measure the total solar irradiance;
- SODISM (SOlar Diameter Imager and Surface Mapper): an imaging telescope accurately pointed and a CCD which allows measuring the solar diameter and

shape with an accuracy of a few milliarc second, and to perform helioseismologic observations to probe the solar interior [5].

## 1.3 MSC Adams

Product manufacturers often struggle to understand true system performance until very late in the design process. Mechanical, electrical, and other subsystems are validated against their specific requirements within the systems engineering process, but full-system testing and validation comes late, leading to rework and design changes that are riskier and more costly than those made in the early stages.
In this vein, MSC Adams software for Multibody Dynamics (MBD) improves engineering efficiency and reduces product development costs by enabling early system-level design validation. MSC Adams makes it possible to evaluate the complex interactions due to the movement of structures in a multi-body system. By including this issue in the design, products can be optimised in terms of performance, safety and comfort. In addition to extensive analysis capabilities, MSC Adams is optimised for large-scale problems, taking advantage of high computing performance.
Utilizing multi-body dynamics solution technology, MSC Adams runs nonlinear dynamics in a fraction of the time required by Finite Element Analysis (FEA) solutions. Finally, MSC Adams can estimate the loads and forces acting on the parts of a multi-body system with greater accuracy than FEA [6].

### 1.3.1 Adams Solver

This software enables the analysis of multi-body systems consisting of rigid and/or flexible bodies. The user provides as input both the geometry of the body and the motion laws and/or forces acting on the system. Then, by solving differential and flexible equations, the software returns as output displacements, velocities, accelerations, forces, torques, stresses, deformations and whatever the user desires, within the non-linear field too. All the parts constituting the multi-body system are linked through ideal joints (inviolable algebraic equations) or elastic joints (more realistic, governed by elastic-viscous equations and modelled in terms of stiffness, friction, damping, etc.). Thus, the combination of bodies, joints and forces represents the multi-body system, whose dynamics is simulated by MSC Adams solving the Euler-Lagrangian equation for the multi-body system [7]:

$$\frac{d}{dt}\frac{\partial \mathscr{L}}{\partial \dot{q}_i} - \frac{\partial \mathscr{L}}{\partial q_i} - \mathcal{Q}_i + \sum_{k=1}^{m} \frac{\partial \phi_k}{\partial q_i}\lambda_k = 0, \quad i = 1, ..., 6 \tag{1.1}$$

where:

- $\mathscr{L}$ is either kinetic or potential energy of the system;

- $q$ are the generalized Lagrangian coordinates of the system;
- $\mathcal{Q}$ are the generalized Lagrangian forces;
- $\phi$ is the constraint function;
- $\lambda_k$ are the Lagrangian multipliers;
- $m$ is the number of constraint equations;
- $i = 1, ..., 6$ indicates the translational and rotational components.

At every single calculation step the code verifies that the solution is within an acceptable error (tolerance) defined by the user; if the error results to be higher than the threshold, the code repeats the calculation with different algorithms till it reaches a numerical convergence or not, informing the user about what went wrong (for example modelling problems or inappropriate parameters for the ongoing analysis).
Finally, the flexibility of the structures can be included within the model, allowing the structural analysis of the system to be performed. The resulting equation is the classical dynamics equation, enriched with a new term. In particular, the terms that appear within this equation are as follows [8]:

- A term with the mass matrix associated to accelerations;
- A term with the stiffness matrix associated to the generalized coordinates;
- A term with the damping matrix associated to the first derivative of the coordinates;
- A term representing the forces;
- A term representing the constraints;
- A new term, with respect to the rigid case which includes all the previous terms, highlighting that changing the body shape, the inertia distribution changes.

Optional modules available with Adams allow users to integrate mechanical components, pneumatics, hydraulics, electronics, and control systems technologies to build and test virtual prototypes that accurately account for the interactions between these subsystems [6].

### 1.3.2 Adams Controls and Adams Mechatronics

Adams Mechatronics is a plug-in to MSC Adams which can be used to easily incorporate control systems into mechanical models. Adams Mechatronics has been developed based on the Adams Controls functionality and contains modeling elements which transfer information to/from the control system. For example, the use of Adams Mechatronics in Adams Car allows to [6]:

- Add a sophisticated controls representation to a MSC Adams model;
- Connect a MSC Adams model to block diagram models developed with control applications such as Easy5 or MATLAB;
- Experience flexibility in simulation styles to suit problems' needs: it simulates within MSC Adams, within the controls software or co-simulation;
- Access advanced pre-processing for Adams Controls;
- Setup and couple a control system to a mechanical system;
- Convert signal units automatically;
- Connect transducer and actuator signals to the control systems easily;
- Conveniently review and modify the control system input and output specifications;
- Deal with complex integrations.

### 1.3.3 Adams Flex and Adams Viewflex

Adams Flex provides the technology to correctly include a component's flexibility even in presence of large overall motion and complex interaction with other modeling elements. Greater emphasis has been placed these days on high-speed, lightweight, precise mechanical systems. Often these systems will contain one or more structural components where deformation effects are paramount for design analyses and the rigid body assumption is no longer valid. Adams Flex allows importing finite element models from most major FEA software packages and is fully integrated with MSC Adams package providing access to convenient modeling and powerful post-processing capabilities. Thanks to this tool it is possible to [6]:

- Integrate FEA-based flexible bodies into a model;
- Better represent structural compliance;
- Predict loads and displacements with greater accuracy;

- Examine the linear system modes of a flexible model;
- Broad and convenient control over modal participation and damping.

The ViewFlex module in Adams View enables users to transform a rigid part to an MNF-based flexible body using embedded finite element analysis where a meshing step and linear modes analysis will be performed. It allows to [6]:

- Create flexible bodies entirely within Adams View or Adams Car;
- Reduce reliance on third party FEA software using built in MSC Nastran technology;
- Generate a flexible body from existing solid geometry, imported meshes or newly created extrusion geometry;
- Obtain detailed control over mesh, modal analysis and flexible body attachment settings for an accurate representation of component flexibility.

### 1.3.4 Adams Durability

Durability testing is a critical aspect of product development and issues discovered late in the development cycle lead to project delays and budget overruns. Worse yet, “in service” failures lead to dissatisfied customers, safety issues, and warranty costs. Adams Durability allows engineers to assess the stresses and durability of mechanical system components to design products that will last. Direct access to physical test data in industry-standard file formats enables engineers to use loads data captured during tests, and to easily correlate simulation and testing results. It allows to [6]:

- Shorten the development cycle, reducing costly durability testing;
- Provide direct file input and output in RPC III and DAC formats to reduce disk space requirements and improve performance;
- Perform modal stress recovery of flexible bodies within MSC Adams;
- Export loads to popular FEA software including MSC Nastran for detailed stress analysis;
- Integrate with MSC Fatigue to do component life prediction.

### 1.3.5 Adams Vibration

With Adams Vibration, engineers replace physical tests on shaker devices with virtual prototypes. Noise, vibration, and harshness (NVH) are critical factors in the performance of many mechanical designs but designing for optimum NVH can be difficult. Adams Vibration allows engineers to easily study forced vibration of mechanical systems using frequency domain analysis. It allows to [6]:

- Analyze the forced response of a model in the frequency domain over different operating points;
- Transfer a linearized model from MSC Adams products to Adams Vibration completely and quickly;
- Create input and output channels for vibration analyses;
- Specify frequency domain input functions, such as swept sine amplitude/frequency, power spectral density (PSD), and rotational imbalance;
- Create frequency-based forces;
- Solve for system modes over frequency range of interest;
- Evaluate frequency response functions for magnitude and phase characteristics;
- Animate forced response and individual mode response;
- Tabulate system modal contributions to forced vibration response;
- Tabulate contribution of model elements to kinetic, static, and dissipative energy distribution in system modes;
- Specify direct kinematic inputs;
- Plot Stress/Strain frequency response functions.

## 1.4 Overview of the thesis

This thesis has different parts to be analysed in order to have a complete study of a flexible spacecraft. On one hand a mathematical model of flexible spacecraft already present in literature has been obtained and analysed, on the other hand the same spacecraft has been implemented with more complexity in MSC Adams. Firstly, the attitude dynamics and kinematics of the spacecraft is studied and modelled, including the dynamics of the flexible solar panels. A finite element analysis with MSC Patran/MSC Nastran was required in order to obtain the natural modes, frequencies, and eigenvectors useful for the model implementation. Once the dynamics

model of the flexible spacecraft was completed, the attention was focused on the Attitude Control System (ACS) for a flexible spacecraft, in particular the choice fell on a PD attitude controller. This one has been implemented in MATLAB/Simulink with the goal of achieving the desired orientation, and maintaining the correct attitude even after the disturbances acting on the system. A tuning of the control gains was required to obtain a satisfactory performance. The work is accomplished with the realization and analysis of the spacecraft in MSC Adams, thanks to which a good validation of the mathematical model has been possible. In order to assess the same manoeuvre simulated for the model case, the tool Adams Controls has been used and MSC Adams has been put into communication with MATLAB/Simulink, in which the same PD controller was implemented.
Now a general overview of the thesis is summarized as follows:

- Chapter 2: all the system mathematical models of this thesis are introduced and divided in three main sections: attitude kinematics and dynamics, flexible spacecraft and attitude control;
- Chapter 3: the whole implementation of the spacecraft in MSC Adams is shown, highlighting all the features in terms of bodies, dimensions, materials, connectors, mesh and forces, and presenting the process to put into communication MSC Adams with MATLAB/Simulink;
- Chapter 4: this is the part where the simulation scenario is reported and all the results regarding the previous sections can be found;
- Chapter 5: the conclusions and future works are discussed.

# Chapter 2

# Flexible spacecraft mathematical model

In the following sections the mathematical models of the spacecraft (Fig. 2.1) and the flexible solar panels are discussed. A hybrid approach is used for implementing the main body attitude dynamics, including the solar panels.

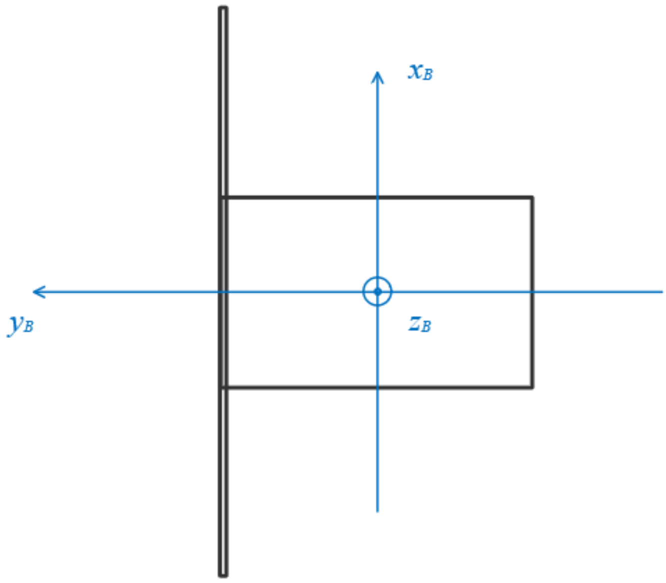


Figure 2.1: The scheme of the spacecraft and flexible solar panels.

## 2.1 Attitude kinematics and dynamics

In this section a discussion about attitude dynamics and kinematics of a rigid body is done. The attitude kinematics of the spacecraft is studied through the quaternions, while Euler's equation is used for the attitude dynamics implementation. After that, a brief overview about internal and external torques acting on the spacecraft is done.

### 2.1.1 Attitude kinematics

The attitude kinematics of the spacecraft is described through Euler parameters, known as quaternions. A quaternion $\mathbf{q}$ is a four-component vector composed by a three-vector part $\mathbf{q}_v$ and scalar part $q_0$:

$$\mathbf{q} = \begin{bmatrix} q_0 \\ \mathbf{q}_v \end{bmatrix} \tag{2.1}$$

where $\mathbf{q}_v = [q_1, q_2, q_3]^T$.
The kinematics equation for the quaternion is in the form [9]:

$$\dot{\mathbf{q}} = \frac{1}{2}\Xi(\mathbf{q})\boldsymbol{\omega} \tag{2.2}$$

where $\Xi(\mathbf{q})$ is defined by:

$$\Xi(\mathbf{q}) = \begin{bmatrix} q_0\boldsymbol{I}_3 + \mathbf{q}_v^x \\ -\mathbf{q}_v^T \end{bmatrix} \tag{2.3}$$

where $\boldsymbol{I}_3 \in \mathbb{R}^{3x3}$ is the identity matrix and $q_v^x \in \mathbb{R}^{3x3}$ is the skew-symmetric matrix:

$$\boldsymbol{q}_v^x = \begin{bmatrix} 0 & -q_3 & q_2 \\ q_3 & 0 & -q_1 \\ -q_2 & q_1 & 0 \end{bmatrix} \tag{2.4}$$

### 2.1.2 Attitude dynamics

The main body is assumed to be a rigid body. The conservation of angular momentum is used to compute the equations for the attitude dynamics of a rigid body [9], known as *Euler's equation*:

$$\dot{\mathbf{H}}_I = \mathbf{M}_I \tag{2.5}$$

In particular, this equation tells that $\mathbf{H}_I$ is constant in absence of any external torques. This equation can be written in a body reference frame, due to the easier expression of the external torques in this frame:

$$\dot{\mathbf{H}}_B = \mathbf{M}_B - \boldsymbol{\omega}_B^{BI} \times \mathbf{H}_B \tag{2.6}$$

where $\boldsymbol{\omega}_B^{BI}$ is the angular velocity of the spacecraft in the body frame. The angular momentum expressed in the body frame is given by:

$$\mathbf{H}_B = \boldsymbol{J}_B \boldsymbol{\omega}_B^{BI} \tag{2.7}$$

where $\boldsymbol{J}_B$ is the moment of inertia expressed in the body frame. Combining (2.6) with (2.7), *Euler's rotational equation* is obtained:

$$\dot{\boldsymbol{\omega}}_B^{BI} = (\boldsymbol{J}_B)^{-1}[\mathbf{M}_B - \boldsymbol{\omega}_B^{BI} \times (\boldsymbol{J}_B \boldsymbol{\omega}_B^{BI})] \tag{2.8}$$

When a set of principal axes is chosen as the body axes, the inertia tensor $\boldsymbol{J}_B$ is diagonal [10] :

$$\boldsymbol{J}_B = \begin{bmatrix} J_x & 0 & 0 \\ 0 & J_y & 0 \\ 0 & 0 & J_z \end{bmatrix} \tag{2.9}$$

The Euler's equation of motion for a rigid body are given by:

$$\begin{cases} J_x\dot{\omega}_1 + (J_z - J_y)\omega_2\omega_3 = M_x \\ J_y\dot{\omega}_2 + (J_x - J_z)\omega_3\omega_1 = M_y \\ J_z\dot{\omega}_3 + (J_y - J_x)\omega_1\omega_2 = M_z \end{cases} \tag{2.10}$$

Eq.(2.8) and the quaternion kinematics equation (2.2) provide a complete description of the motion of a rigid body [9].

### Internal torques

The spacecraft is constituted by several parts connected by joints and cannot be considered as a single rigid body. There are internal torques acting on the spacecraft, due to the presence of reaction wheels (RWs), control moment gyros (CMGs), the flexibility of some bodies of the spacecraft, or the slosh of liquid fluids. In this section the reaction wheels dynamics is discussed. Reaction wheels are known as *momentum exchange* devices, due to the capability to generate internal torques to the spacecraft without changing the overall angular momentum. In this case a system of three reaction wheels is considered. The RWs system is modelled with a first order filter and a saturation block for each wheel in Simulink environment (Fig.

2.2). The reaction wheels are subjected to two limitations: a torque saturation, due to the maximum torque that the wheels can provide for electrical limitation, and a momentum saturation, due to a mechanical limitation. When the wheel reaches the maximum velocity, it is not able to further accelerate and "desaturation" with reaction control thrusters or magnetotorquers is needed.

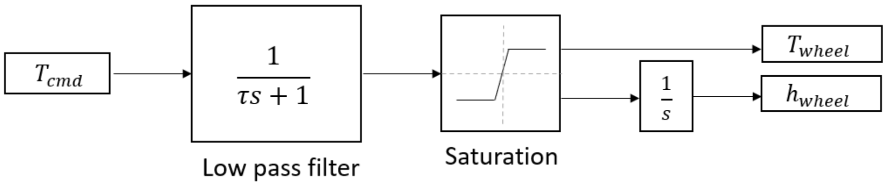


Figure 2.2: Reaction wheels model [3].

The reaction wheels block has the required control torque from the controller as input, and gives the reaction wheels torque (2.11) and momentum (2.12) as output:

$$T_{wheel_i} = -\frac{1}{\tau s + 1} \cdot T_{cmd_i} \tag{2.11}$$

$$h_{wheel_i} = \frac{1}{s} \cdot T_{wheel_i} \tag{2.12}$$

where $i = 1, ..., n_a$, with $n_a$ equal to the number of actuators. The three reaction wheels are set in a very standard gyroscopic configuration at the center of mass of the spacecraft acting along the three body axes, as in Fig. 2.3.

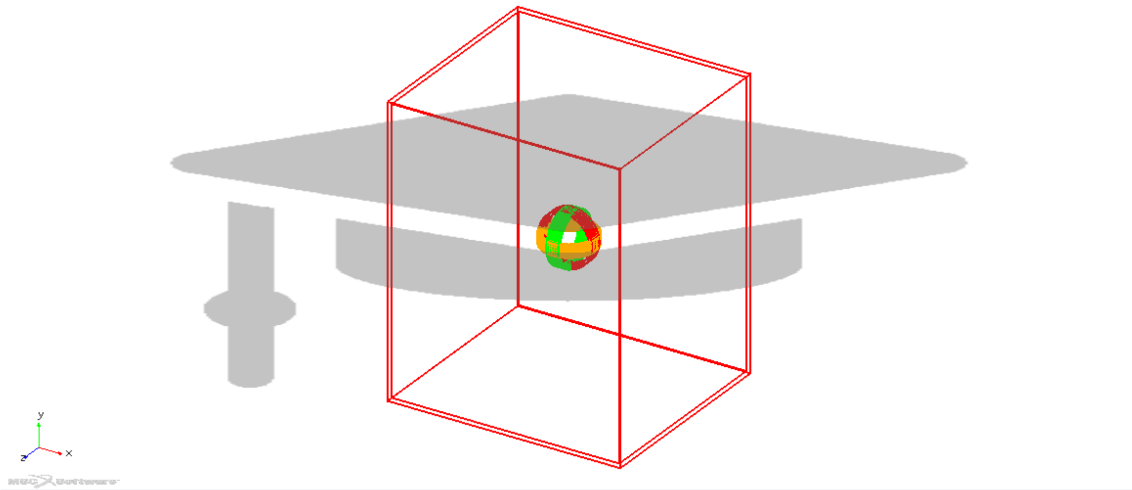


Figure 2.3: Reaction wheels configuration from MSC Adams.

The final expressions for the torque and angular momentum of the reaction wheels are given by:

$$\boldsymbol{M}_{rws} = \begin{bmatrix} T_{wheel_1} \\ \vdots \\ T_{wheel_{na}} \end{bmatrix} \tag{2.13}$$

$$\boldsymbol{H}_{rws} = \begin{bmatrix} h_{wheel_1} \\ \vdots \\ h_{wheel_{na}} \end{bmatrix} \tag{2.14}$$

The generalization of the Euler's equation (2.8), including the reaction wheels, is given by:

$$\dot{\boldsymbol{\omega}}_B^{BI} = (\boldsymbol{J}_B)^{-1}[\mathbf{M}_B - \mathbf{M}_B^{rws} - \boldsymbol{\omega}_B^{BI} \times (\boldsymbol{J}_B\boldsymbol{\omega}_B^{BI} + \boldsymbol{H}_B^{rws})] \tag{2.15}$$

where the angular momentum of the reaction wheels is given by:

$$\boldsymbol{H}_B^{rws} = \boldsymbol{J}_{rws}\boldsymbol{\omega}_{rws} \tag{2.16}$$

with $\boldsymbol{J}_{rws}$ that is the reaction wheels moment of inertia, and $\boldsymbol{\omega}_{rws}$ as the angular velocity. The negative sign before $\boldsymbol{M_B^{rws}}$ on the right side reflects Newton's third law of motion [3].

### External torques

External torques involve the interaction between the spacecraft and the entities external to it. In general a spacecraft is subjected to different perturbations in space, such as gravity gradient, magnetic field, aerodynamic torque or solar radiation pressure torque, due to the space environment. In this case the only external disturbance of the gravity gradient is considered, due to its higher value compared with the other disturbances.
Hence, Eq. (2.14) can be written as follows:

$$\dot{\boldsymbol{\omega}}_B^{BI} = (\boldsymbol{J}_B)^{-1}[\mathbf{M}_{ext} - \mathbf{M}_B^{rws} - \boldsymbol{\omega}_B^{BI} \times (\boldsymbol{J}_B\boldsymbol{\omega}_B^{BI} + \boldsymbol{H}_B^{rws})] \tag{2.17}$$

where $\boldsymbol{M}_{ext}$ is the external disturbance due to the gravity gradient [3].

## 2.2 Flexible Spacecraft

This thesis deals with the problem of the spacecraft with flexible structures. The appendages of a spacecraft consist of lightweight, flexible, deployable solar panels, antennas, or booms [11] (Fig. 2.4). A flexible spacecraft is expected to achieve high pointing and fast attitude manoeuvring, that can introduce levels of vibration to flexible appendages due to the rigid-flexible coupling effect, which can cause the deterioration of its pointing performance [12]. The attitude controllers perform some functions such as pointing the antennas in a desired direction, pointing solar panels towards the sun, keeping sensors and equipment away from the sun's light and heat [11]. Attitude manoeuvres can create significant vibrations in the satellite body. This section aims at modelling the dynamics of the solar panels and the coupling effect between the rigid and flexible parts.


Figure 2.4: Flexible spacecraft appendages [13].

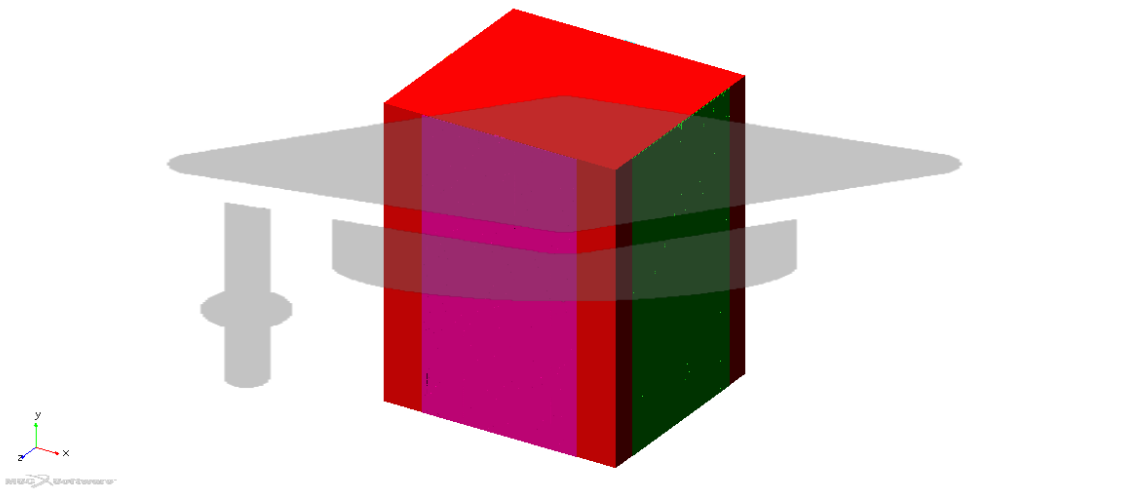


Figure 2.5: Spacecraft in stored configuration in MSC Adams View.

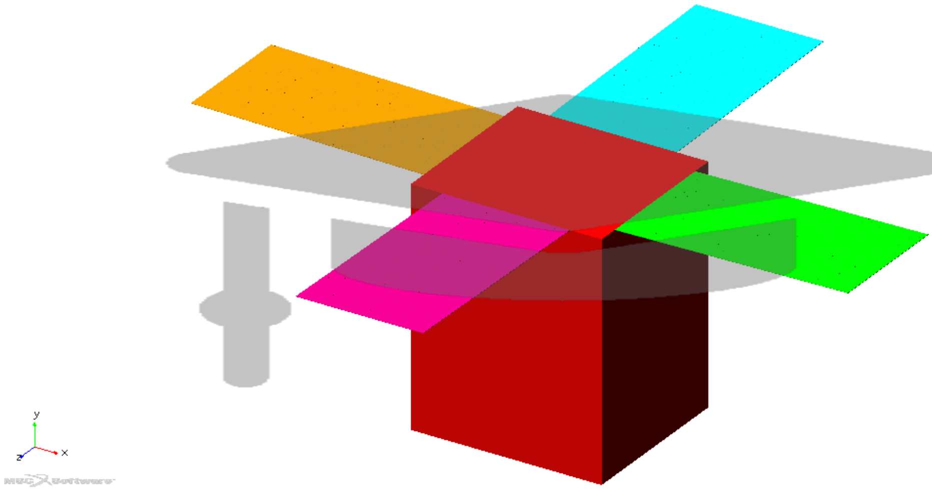


Figure 2.6: Spacecraft in deployed configuration in MSC Adams View.

### 2.2.1 Flexible Spacecraft Dynamics

The flexible part of the spacecraft is represented by the four solar panels (Fig. 2.6). The Euler's equation (2.17) is written including the flexible appendages. The flexible dynamic equations are given by [14]:

$$\boldsymbol{J}\dot{\boldsymbol{\omega}} + \boldsymbol{\delta}^T\ddot{\boldsymbol{\eta}} = \boldsymbol{M}_{ext} + \boldsymbol{M}_{RW} - \boldsymbol{\omega} \times (\boldsymbol{J}\boldsymbol{\omega} + \boldsymbol{H}_{RW} + \boldsymbol{\delta}^T\dot{\boldsymbol{\eta}}) \tag{2.18}$$

$$\ddot{\boldsymbol{\eta}} + \boldsymbol{C}\dot{\boldsymbol{\eta}} + \boldsymbol{K}\boldsymbol{\eta} = -\boldsymbol{\delta}\dot{\boldsymbol{\omega}} \tag{2.19}$$

Eq. (2.18) represents the Euler's equation, including the flexible solar panels, in body reference frame. The rigid dynamics of the total angular momentum is given by [14]:

$$\boldsymbol{\chi} = \boldsymbol{J}\boldsymbol{\omega} + \boldsymbol{\delta}^T\dot{\boldsymbol{\eta}} \tag{2.20}$$

where:

- $\boldsymbol{J}$ represents the symmetric inertia matrix of the whole structure, that is the sum of the main body's inertia matrix $\boldsymbol{J}_{mb}$, positive defined, and a symmetric inertia matrix due to the flexible structure;
- $\boldsymbol{\delta}$ is the coupling matrix between the elastic and rigid structures;
- $\boldsymbol{\eta}$ is the modal coordinate vector.

Eq. (2.19) describes the flexible dynamics, under the assumption of small elastic deformations. $\boldsymbol{K}$ and $\boldsymbol{C}$ are defined as follows:

$$\boldsymbol{K} = diag\left\{\omega_{ni}^2, i = 1, ..., N\right\} \tag{2.21}$$

$$\boldsymbol{C} = diag\left\{2\zeta_i\omega_{ni}, i = 1, ..., N\right\} \tag{2.22}$$

Eqs. (2.21) and (2.22) are respectively the stiffness matrix and the damping matrix. $N$ is the number of elastic modes, $\omega_{ni}$ are the natural frequencies, and $\zeta_i$ are the corresponding damping ratios. In this work, the damping matrix is obtained from the stiffness matrix multiplied by a coefficient $\gamma$:

$$\boldsymbol{C} = \gamma\boldsymbol{K} \tag{2.23}$$

It is indeed not easy to compute the damping ratios without a detailed structural model or a experimental analysis, but this problem is not part of the thesis topics. It is worth noting that the solar panels are four. Therefore, four contributions represented by $\boldsymbol{\delta}_i, i = 1, ..., n_{SAP}$ have to be considered in Euler's equations, with $n_{SAP} = 4$, number of solar panels:

$$\boldsymbol{H}_{SAP} = \sum_{i=1}^{n_{SAP}} \boldsymbol{\delta}_i^T\dot{\boldsymbol{\eta}}_i \tag{2.24}$$

$$\boldsymbol{M}_{SAP} = \sum_{i=1}^{n_{SAP}} \boldsymbol{\delta}_i^T\ddot{\boldsymbol{\eta}}_i \tag{2.25}$$

where $\boldsymbol{H}_{SAP}$ represents the contribution of the flexible parts to the total angular momentum, while $\boldsymbol{M}_{SAP}$ is the contribution to the total disturbance torque acting on the spacecraft. The flexibility of the solar panels included in the model is an internal disturbance with respect to the spacecraft, as in the case of the reaction wheels explained in section (2.1.2). Including Eqs. (2.24) and (2.25) in (2.18), the final expression of Euler's equation becomes:

$$\dot{\boldsymbol{\omega}} = \boldsymbol{J}^{-1}[-\boldsymbol{\omega} \times (\boldsymbol{J}\boldsymbol{\omega} + \boldsymbol{H}_{SAP} + \boldsymbol{H}_{RW}) - \boldsymbol{M}_{SAP} + \boldsymbol{M}_{ext} + \boldsymbol{M}_{RW}] \tag{2.26}$$

$$\ddot{\boldsymbol{\eta}}_i = -\boldsymbol{\delta}_i\dot{\boldsymbol{\omega}} - (\boldsymbol{K}\boldsymbol{\eta}_i + \boldsymbol{C}\dot{\boldsymbol{\eta}}_i), \ \ i = 1, ..., n_{SAP} \tag{2.27}$$

It can be demonstrated that $\boldsymbol{\delta}^T\boldsymbol{\delta}$ represents the contribution of the flexible parts to the total inertia matrix [14]. Therefore, the total inertia matrix of the whole structure, that appears in Eq. (2.26), is defined as follows:

$$\boldsymbol{J} = \boldsymbol{J}_{mb} + \boldsymbol{J}_{SAP} \tag{2.28}$$

where:

$$\boldsymbol{J}_{SAP} = \sum_{i=1}^{n_{SAP}} \boldsymbol{\delta}_i^T \boldsymbol{\delta}_i \tag{2.29}$$

### 2.2.2 Coupling matrix

A particular attention is given to the interaction between spacecraft attitude control systems and flexible structures. The traditional assumption considers that the dynamic response to attitude control devices is uncoupled from vehicle vibrations, but some appendages cannot be designed with sufficient rigidity to justify it [15]. Therefore, it is necessary to compare the coupled equations of vibration with the attitude dynamics given by Euler's equation. This section is dedicated to the computation of the coupling matrix $\boldsymbol{\delta}$ between the flexible and rigid structures of the spacecraft, that appears in Eqs. (2.18) and (2.19). As reported in [2], the coupling matrix is defined as the following N by 3 matrix:

$$\bar{\boldsymbol{\delta}} = -\boldsymbol{\phi}^T \boldsymbol{M}(\boldsymbol{\Sigma}_{0E} - \boldsymbol{\Sigma}_{E0}\widetilde{\boldsymbol{R}} - \tilde{\boldsymbol{r}}\boldsymbol{\Sigma}_{E0}) \tag{2.30}$$

where [2, 15]:

- $\boldsymbol{\delta}$ is the coupling matrix $6n \times 3$, with $n$ equal to the number of sub-bodies in which each panel is divided. The bar over $\delta$ indicates that it is a truncated matrix of dimensions $N \times 3$, with $N$ equal to the number of appendages modal coordinates retained after truncation, or the normal modes;
- $\boldsymbol{\phi}$ represents the matrix of the eigenvectors of the appendages of dimensions $6n \times 6n$. Also in this case, the bar over $\boldsymbol{\phi}$ indicates the truncation of the eigenvectors matrix, defined as a $6n \times N$ matrix;
- $\boldsymbol{M}$ is a $6n \times 6n$ matrix of masses and inertias of appendages sub-bodies;
- $\boldsymbol{\Sigma}_{0E}$ and $\boldsymbol{\Sigma}_{E0}$ are $6n \times 3$ matrix operators;
- $\boldsymbol{R}$ is a $3 \times 1$ matrix, defined below. The $(\sim)$ operator indicates the skew-symmetric $3 \times 3$ matrix.
- $\tilde{\boldsymbol{r}}$ is a $6n \times 6n$ matrix, defined below.

For simplicity, the bar over $\boldsymbol{\delta}$ and $\boldsymbol{\phi}$ truncated matrices is omitted. Now the matrices in all the matrices in Eq. (2.30) are defined. Before that, it is important to remember that $n$ represents the total number of rigid bodies in a discrete parameter model of an appendage, as shown in Fig. 2.7.

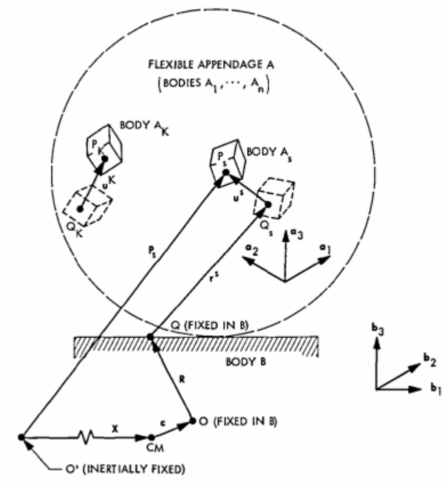


Figure 2.7: Discrete-parameter appendage sub-body coordinates [2].

In this work, it is assumed $n = 9$, hence each of the four solar panels has been divided into nine sub-panels, as shown in Fig. 2.8, where, for simplicity, the division of only one solar panel is represented.

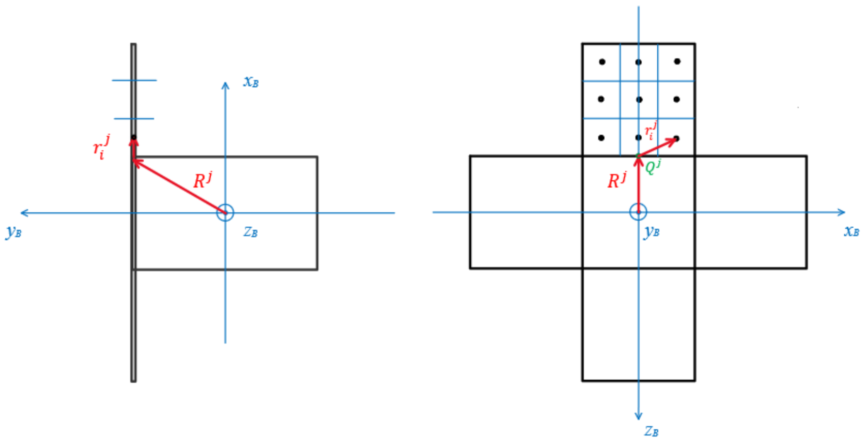

Figure 2.8: Front and upper view of spacecraft with sub-panels division.

The $\boldsymbol{M}$ matrix is defined in terms of $3 \times 3$ partitioned matrices:

$$
\boldsymbol{M} = \begin{bmatrix} \boldsymbol{m}^1 & 0 & 0 & 0 & ... & 0 & 0 \\ 0 & \boldsymbol{I}^1 & 0 & 0 & ... & 0 & 0 \\ 0 & 0 & \boldsymbol{m}^2 & 0 & ... & 0 & 0 \\ 0 & 0 & 0 & \boldsymbol{I}^2 & ... & 0 & 0 \\ \vdots & \vdots & \vdots & \vdots & \vdots\vdots\vdots & \vdots & \vdots \\ 0 & 0 & 0 & 0 & ... & \boldsymbol{m}^n & 0 \\ 0 & 0 & 0 & 0 & ... & 0 & \boldsymbol{I}^n \end{bmatrix} \tag{2.31}
$$

For example, in the specific case of $n = 1$, the $\boldsymbol{M}$ matrix becomes:

$$
\boldsymbol{M}_1 = \begin{bmatrix} \boldsymbol{m}^i & 0 \\ 0 & \boldsymbol{I}^i \end{bmatrix} = \begin{bmatrix} m_1 & 0 & 0 & 0 & 0 & 0 \\ 0 & m_1 & 0 & 0 & 0 & 0 \\ 0 & 0 & m_1 & 0 & 0 & 0 \\ 0 & 0 & 0 & I_{x1} & 0 & 0 \\ 0 & 0 & 0 & 0 & I_{y1} & 0 \\ 0 & 0 & 0 & 0 & 0 & I_{z1} \end{bmatrix} \tag{2.32}
$$

where $\boldsymbol{m}^i = m_i\boldsymbol{E}$, with $\boldsymbol{E}$ equal to the identity matrix, and $\boldsymbol{I}^i$ represents the sub-panel inertia tensor with respect to the sub-panel CoM. The $\boldsymbol{M}^j$ matrix in the case of $n = 9$ sub-panels becomes:

$$
\boldsymbol{M}^j = \begin{bmatrix} m_1 & 0 & 0 & 0 & 0 & 0 & ... & 0 & 0 & 0 & 0 & 0 & 0 \\ 0 & m_1 & 0 & 0 & 0 & 0 & ... & 0 & 0 & 0 & 0 & 0 & 0 \\ 0 & 0 & m_1 & 0 & 0 & 0 & ... & 0 & 0 & 0 & 0 & 0 & 0 \\ 0 & 0 & 0 & I_{x1} & 0 & 0 & ... & 0 & 0 & 0 & 0 & 0 & 0 \\ 0 & 0 & 0 & 0 & I_{y1} & 0 & ... & 0 & 0 & 0 & 0 & 0 & 0 \\ 0 & 0 & 0 & 0 & 0 & I_{z1} & ... & 0 & 0 & 0 & 0 & 0 & 0 \\ \vdots & \vdots & \vdots & \vdots & \vdots & \vdots & \vdots\vdots\vdots & \vdots & \vdots & \vdots & \vdots & \vdots & \vdots \\ 0 & 0 & 0 & 0 & 0 & 0 & ... & m_n & 0 & 0 & 0 & 0 & 0 \\ 0 & 0 & 0 & 0 & 0 & 0 & ... & 0 & m_n & 0 & 0 & 0 & 0 \\ 0 & 0 & 0 & 0 & 0 & 0 & ... & 0 & 0 & m_n & 0 & 0 & 0 \\ 0 & 0 & 0 & 0 & 0 & 0 & ... & 0 & 0 & 0 & I_{xn} & 0 & 0 \\ 0 & 0 & 0 & 0 & 0 & 0 & ... & 0 & 0 & 0 & 0 & I_{yn} & 0 \\ 0 & 0 & 0 & 0 & 0 & 0 & ... & 0 & 0 & 0 & 0 & 0 & I_{zn} \end{bmatrix} \tag{2.33}
$$

where the index $j = 1, ..., n_{SAP}$ represents the number of solar panels.

In general, $\boldsymbol{\Sigma}_{E0}$ and $\boldsymbol{\Sigma}_{0E}$ are defined as follows:

$$\boldsymbol{\Sigma}_{E0} = \begin{bmatrix} \boldsymbol{E} \\ \boldsymbol{0} \\ \vdots \\ \boldsymbol{E} \\ \boldsymbol{0} \end{bmatrix}, \quad \boldsymbol{\Sigma}_{0E} = \begin{bmatrix} \boldsymbol{0} \\ \boldsymbol{E} \\ \vdots \\ \boldsymbol{0} \\ \boldsymbol{E} \end{bmatrix} \tag{2.34}$$

where:

$$\boldsymbol{E} = \begin{bmatrix} 1 & 0 & 0 \\ 0 & 1 & 0 \\ 0 & 0 & 1 \end{bmatrix}, \quad \boldsymbol{0} = \begin{bmatrix} 0 & 0 & 0 \\ 0 & 0 & 0 \\ 0 & 0 & 0 \end{bmatrix} \tag{2.35}$$

For $n = 9$, $\boldsymbol{\Sigma}_{E0}$ and $\boldsymbol{\Sigma}_{0E}$ are composed by these $3 \times 3$ matrices repeated $n$ times.

The term $\boldsymbol{R}$ represents the vector from the CoM of the spacecraft to the jth-point $Q^j$, , with $j = 1, ..., n_{SAP}$. It is important to remember that in Eq.(2.30) all the matrices are expressed in the body-frame.
For $\boldsymbol{R} = [R_1, R_2, R_3]^T$. the term $\widetilde{\boldsymbol{R}}$ that appears in Eq.(2.30) is the corresponding skew-matrix:

$$\widetilde{\boldsymbol{R}} = \begin{bmatrix} 0 & -R_3 & R_2 \\ R_3 & 0 & -R_1 \\ -R_2 & R_1 & 0 \end{bmatrix} \tag{2.36}$$

For the computation of the matrix $\widetilde{\boldsymbol{r}}$, the solar panels frames in Fig. 2.9 are considered. The $\boldsymbol{r}_i^j$ vectors go from point $Q^j$, that represents the central joint between the main body and each solar panel, and the CoM of each sub-panel (Fig. 2.8). It is worth noting that, after the computation of these vectors in each solar panel frame, they have to be transformed in the body reference frame.

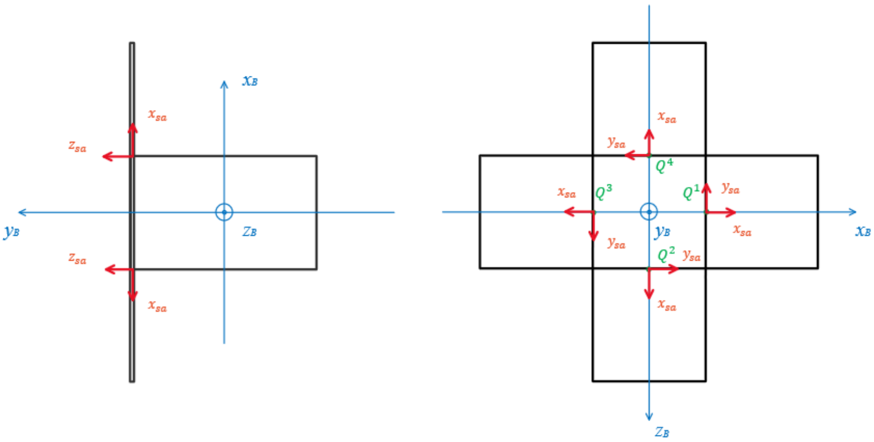


Figure 2.9: Solar panels reference frames.

In general the vector $\boldsymbol{r}$ and the corresponding $\tilde{\boldsymbol{r}}$ that appears in Eq. (2.30) are defined as follows:

$$\boldsymbol{r} = \begin{bmatrix} \boldsymbol{r}_1 \\ 0 \\ \boldsymbol{r}_2 \\ 0 \\ \vdots \\ \boldsymbol{r}_n \\ 0 \end{bmatrix} \tag{2.37}$$

$$\tilde{\boldsymbol{r}} = \begin{bmatrix} \tilde{\boldsymbol{r}}_1 & 0 & 0 & 0 & \dots & 0 & 0 \\ 0 & 0 & 0 & 0 & \dots & 0 & 0 \\ 0 & 0 & \tilde{\boldsymbol{r}}_2 & 0 & \dots & 0 & 0 \\ 0 & 0 & 0 & 0 & \dots & 0 & 0 \\ \vdots & \vdots & \vdots & \vdots & \vdots\vdots\vdots & \vdots & \vdots \\ 0 & 0 & 0 & 0 & \dots & \tilde{\boldsymbol{r}}_n & 0 \\ 0 & 0 & 0 & 0 & \dots & 0 & 0 \end{bmatrix} \tag{2.38}$$

where each term $\tilde{\boldsymbol{r}}_i$, for $i = 1, ..., n$, is the corresponding $3 \times 3$ skew-matrix.

Finally, the last term of Eq. (2.30) to be defined is the $6n \times 6n$ matrix of eigenvectors $\boldsymbol{\phi}$. In order to evaluate the eigenvectors for each solar panel, a Finite Element Method (FEM) analysis is done. For a complete explanation of this analysis, refer to the next section [3].

### 2.2.3 FEM analysis

A significant aspect of this thesis is the FEM analysis conducted with MSC Patran/MSC Nastran software. This analysis is necessary in order to evaluate the natural modes and frequencies that appear in the stiffness and damping matrices (Eqs.(2.21) and (2.22)), and the eigenvectors. The geometry is realized in MSC Patran (Fig. 2.10), with a central surface that represents the top part of the satellite, and the four surfaces for the solar panels. The panels are modelled as aluminium plates with the 2D shell property. The body is assumed to be rigid, and the four surfaces are connected to it through a fixed constraint. In Fig. 2.10, it can be noted a mesh with quad-elements. In order to obtain the values mentioned before, a modal analysis is done using the solver MSC Nastran, and the post-processor of MSC Patran for the results.

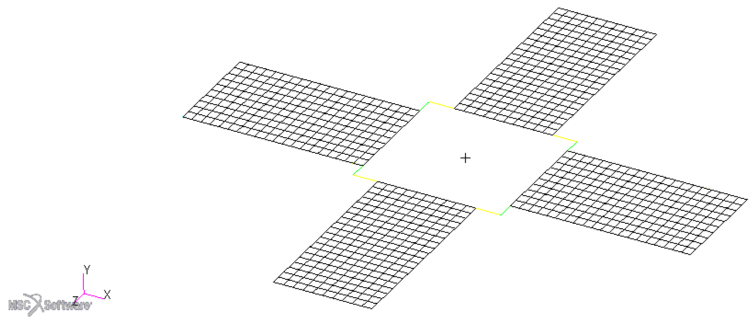


Figure 2.10: Solar panels model in MSC Patran.

From these analysis, it is expected to obtain the shape modes in Fig. 2.11 for each solar panel, in the case of a fixed joint.

For the computation of the natural frequencies of the model, the approximate Raleigh-Ritz Method reported in [17] can also be used. According to this method, the natural frequencies in $[rad/s]$ of a cantilever plate of dimensions $a \times b \times h$ can be expressed by:

$$\omega_n = \frac{\lambda_n}{a^2}\sqrt{\frac{D}{\rho n}} \tag{2.39}$$

where $D = Eh^3/[12(1-\nu^2)]$ is the flexural rigidity of the plate, $E$ is the Young's Modulus, $\nu$ is the Poisson's ratio, and $\rho$ is the mass density. Known the aspect ratio (b/a), the value of the frequency parameter $\lambda$ can be obtained, and from it the natural frequencies.

Finally, a discussion about the eigenvectors matrix $\boldsymbol{\phi}$ can be done. As explained in section (2.2.1), the damping matrix is chosen after knowing the stiffness matrix, hence the FEM analysis is done without including the damping coefficient.

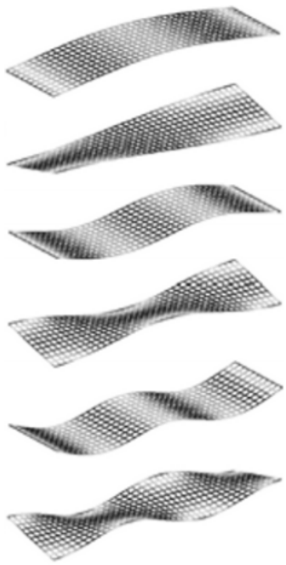

Figure 2.11: First six modes of a solar panel fixed to a satellite [16].

In general, the free vibration of motion for a linear and undamped structure may be expressed in the matrix notation [17]:

$$\boldsymbol{M}\ddot{\boldsymbol{u}} + \boldsymbol{K}\boldsymbol{u} = \boldsymbol{0} \tag{2.40}$$

where $\boldsymbol{M}$ is the mass matrix, $\boldsymbol{K}$ is the stiffness matrix, $\boldsymbol{u}$ is the displacement vector. For a linear system, free vibrations are harmonic, and can be expressed in the form:

$$\boldsymbol{u} = \boldsymbol{\phi} \sin \omega t \tag{2.41}$$

where $\boldsymbol{\phi}$ is the eigenvector or mode shape, and $\omega$ is the natural frequency. Substituting this equation in Eq.(2.40), and after simplifying, the equation becomes:

$$(\boldsymbol{K} - \boldsymbol{\omega}_i^2 \boldsymbol{M})\boldsymbol{\phi} = 0 \tag{2.42}$$

that is also known as the eigenvalues problem.
In general, when a linear elastic structure is vibrating in free or forced vibration, its deflected shape at any given time is a linear combination of all of its normal modes [18]

$$\boldsymbol{u} = \sum_i \boldsymbol{\phi}_i \boldsymbol{\xi}_i \tag{2.43}$$

where $\boldsymbol{u}$ is the vector of physical displacements, $\boldsymbol{\phi}_i$ is the i-th mode shape, and $\boldsymbol{\xi}_i$ is the modal displacement.

Through the FEM analysis software, it is possible to obtain the eigenvectors for this model. The eigenvectors matrix $\boldsymbol{\phi}$ can be defined as follows:

$$\boldsymbol{\phi}_n^N = \begin{bmatrix} \phi_1^1 & \phi_2^1 & \dots & \phi_n^1 \\ \phi_1^2 & \phi_2^2 & \dots & \phi_n^2 \\ \vdots & \vdots & \vdots\vdots\vdots & \vdots \\ \phi_1^N & \phi_N^2 & \dots & \phi_n^N \end{bmatrix} \tag{2.44}$$

where $n$ is the number of sub-panels each panel is divided in, and $N$ is the number of shape modes. For the definition of the eigenvectors matrix, the eigenvectors of the nodes corresponding to the CoM of each sub-panels are considered. For each node and for a $N-th$ shape mode, a $\boldsymbol{\phi}_i$ matrix, for $i = 1, ..., n$, is defined:

$$\boldsymbol{\phi}_i = [T_1, T_2, T_3, R_1, R_2, R_3] \tag{2.45}$$

where $T_1, T_2, T_3$ are the translational eigenvectors, and $R_1, R_2, R_3$ are the rotational eigenvectors obtained by the modal analysis with MSC Patran/MSC Nastran [3].

## 2.3 Attitude control

In order to regulate the attitude of the spacecraft, a simple Proportional-Derivative (PD) controller is adopted, aiming at reaching the desired angular position.

### 2.3.1 PID controller

PID controllers are the most employed controllers in industrial field due to their capability to provide a satisfactory performance for many control problems [19]. The logic of the PID controller lies in the propagation of a weighted sum of the input signal, its integral, and its first derivative to the output [20]. The output signal in the time domain is given by:

$$y(t) = k_P \cdot x(t) + k_I \cdot \int x(t)dt + k_D \cdot \frac{dx(t)}{dt} \tag{2.46}$$

The input to the PID controller is the control error $\varepsilon(t)$, given by the difference between the reference signal and the actual signal measured by the sensors, as shown in Fig. 2.12. In the Laplace domain the transfer function is given by:

$$\frac{Y(s)}{X(s)} = k_P + \frac{k_I}{s} + k_D s = \frac{k_D s^2 + k_P s + k_I}{s} \tag{2.47}$$

The constants $k_P, k_I$ and $k_D$ are adjustable and optimized for the specific type of process and control goal.

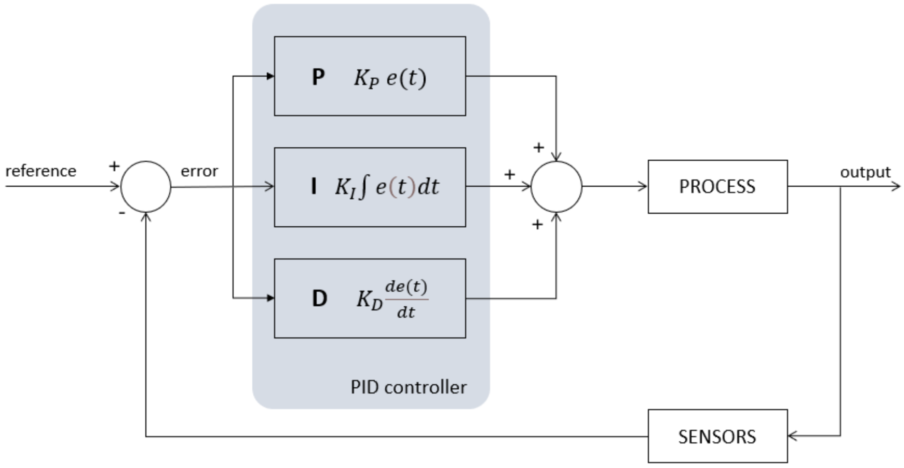


Figure 2.12: Block diagram of a PID controller [3].

*Proportional component*
A high proportional term $k_P$ can lead to a low sensibility, small steady-state error, and good disturbance rejection. On the other hand, $k_P$ has some upper limits, either physical or related to stability and overshoot.

*Integral component*
The integral component $k_I$ is responsible for eliminating the steady-state error. Indeed, if the input of the PID controller is the control error $\varepsilon$, then the integrator component changes the corrective action until $\varepsilon = 0$. Compared to $k_P$, the integral component is kept relatively small, due to undesirable transient responses, overshoot increase, and even instability.

*Derivative component*
The derivative component $k_D$ helps providing a rapid transient response. If a transient disturbance or a sudden change of the set-point occurs, then the first derivative is huge, and causes a correspondingly strong control action [20]. The derivative component also contributes to the increase of the system's stability.

Tab. 2.1 resumes the consequences of the increase of each PID gain [21].

Table 2.1: PID gains

| | Rise Time | Overshoot | Settling Time | Steady State Error | Stability |
|---|---|---|---|---|---|
| $k_P \uparrow$ | decrease | increase | small increase | decrease | degrade |
| $k_I \uparrow$ | small decrease | increase | increase | large decrease | degrade |
| $k_D \uparrow$ | small decrease | decrease | decrease | minor change | improve |

# Chapter 3

# Spacecraft implementation through MSC Adams

## 3.1 Design implementation

In this section the whole design implementation of the spacecraft in MSC Adams environment is shown and explained, clarifying which kind of simplifications and/or differences have been introduced with respect to the Picard satellite, in terms of bodies dimensions, materials, joints, forces and torques used to define the system.

### 3.1.1 Bodies

The spacecraft is composed of:

- One central rigid main body or hub (Fig. 3.1);
- Four flexible solar panels (Fig. 3.2);
- Three reaction wheels at the CoM of the system, acting along the three body axes (Fig. 3.3).

All these parts are made of aluminium. It is worth to notice that, since a big block of aluminium as hub would have been too heavy, it has been decided to design the main body like a shell with a thickness of 1 cm for all the three dimensions, in order to be within a certain range of weight as more as possible. All bodies specifications are reported in Tab. 3.1:

Table 3.1: Bodies specifications

| | Specifications |
|---|---|
| Spacecraft main body | Size: 0.9 m x 1.1 m x 0.8 m [4]<br>Mass: 138.88512 Kg<br>Material: aluminium<br>Euler Modulus: $7.1705 \cdot 10^{10}$ $N/m^2$<br>density: 2740 $Kg/m^3$<br>Poisson ratio: 0.33<br>Moments of inertia in body frame:<br>$I_x = 34.140277248$ $Kg/m^2$<br>$I_y = 28.156643328$ $Kg/m^2$<br>$I_z = 36.784881408$ $Kg/m^2$ |
| Solar Array Panels (SAP) | Size of each SAP: 0.6 m x 1.098 m x 0.002 m<br>Mass of each SAP: 3.610224 Kg<br>Material: aluminium<br>Euler Modulus: $7.1705 \cdot 10^{10}$ $N/m^2$<br>Density: 2740 $Kg/m^3$<br>Poisson ratio: 0.33<br>Moments of inertia in body frame:<br>$I_x = 0.3628948561$ $Kg/m^2$<br>$I_y = 0.1085496589$ $Kg/m^2$<br>$I_z = 0.4714373016$ $Kg/m^2$ |
| Reaction wheels | Size of each wheel:<br>Inner radius: 0.093 m<br>Outer radius: 0.103 m<br>Length: 0.046 m<br>Mass of each wheel: 0.7760940226 Kg<br>Material: aluminium<br>Euler Modulus: $7.1705 \cdot 10^{10}$ $N/m^2$<br>density: 2740 $Kg/m^3$<br>Poisson ratio: 0.33<br>Moment of inertia: $7.4730093436 \cdot 10^{-3}$ $Kg/m^2$<br>Max. angular momentum : 0.4 $Nms$ [22]<br>Max. torque: 0.1 $Nm$ [22] |

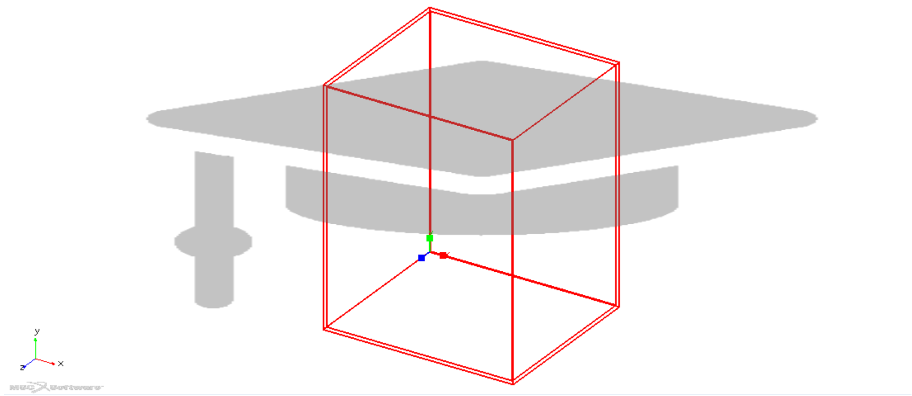

Figure 3.1: Hub

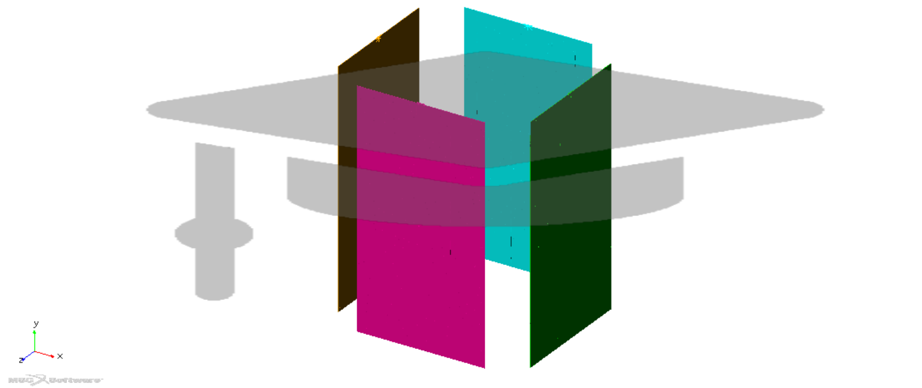

Figure 3.2: Solar panels

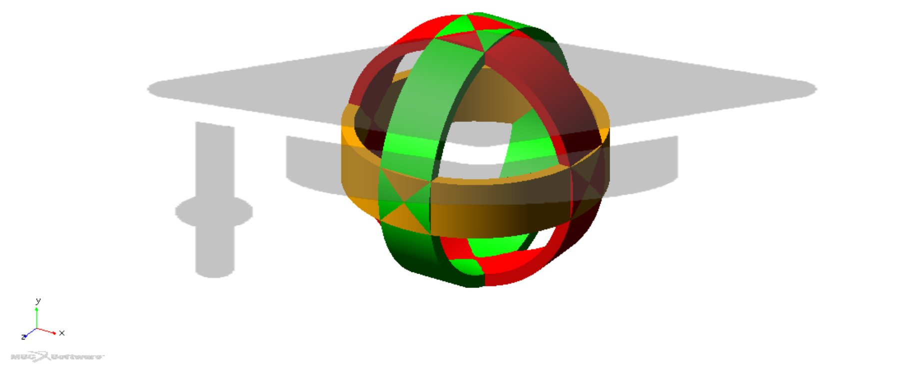

Figure 3.3: Reaction wheels

Each solar panel has been made flexible through the creation of .mnf files, where all FEM informations are reported.
Specifications about the mesh used for this model are reported in Tab. 3.2:

| Element type | Solid tetrahedral |
|---|---|
| Number of element faces | 40010 |
| Number of elements | $\approx$ 10000 |
| Number of nodes | 3493 |

Table 3.2: FEM specifications

Some of the first system modes, generated by the influence of all the parts constituting the spacecraft, showing the first and second flexional and the first and second torsional modes of the panels are reported in Fig. 3.4:

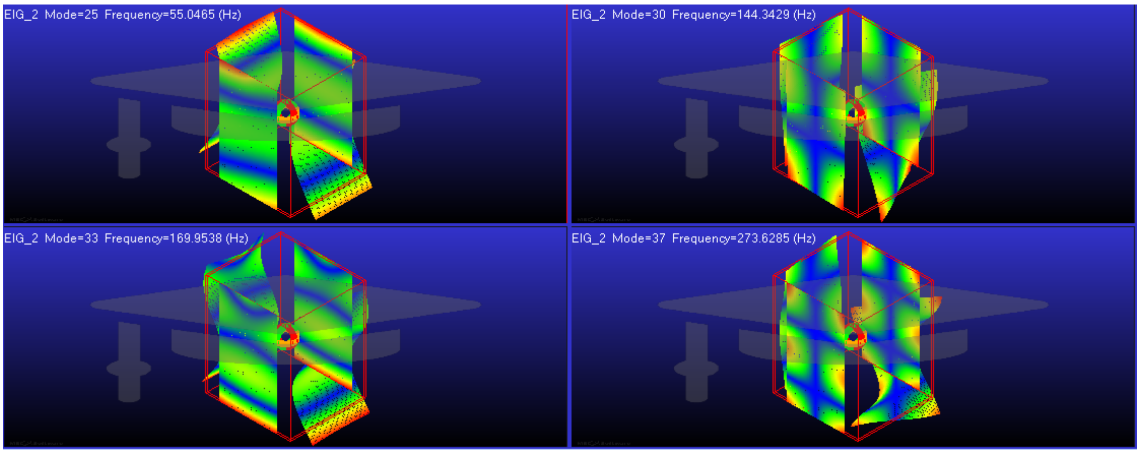


Figure 3.4: Some first system modes.

The strength of MSC Adams is that it manages to carry out non-linear analysis. In fact, when the system behaves in a non-linear way, the frequencies change instant by instant and at every different moment different modes take action.

### 3.1.2 Connectors

Each solar panel is linked to the main body structure through a revolute joint (hinge), type of connector that allows only one degree of freedom (DoF), i.e. the rotation about the rotational axis of each hinge (Fig. 3.5).

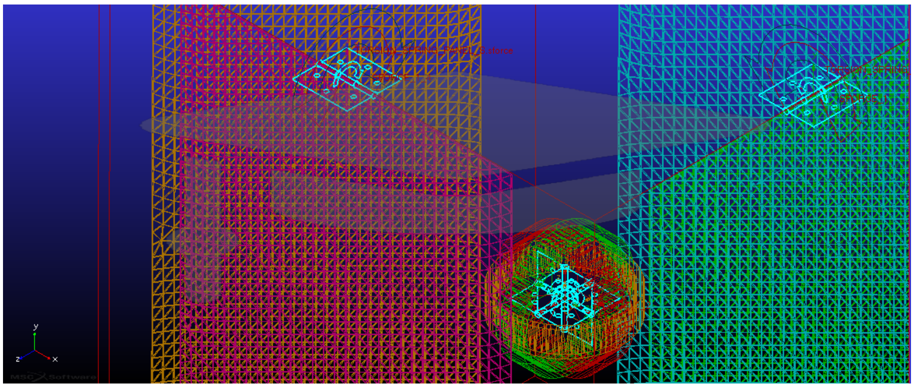


Figure 3.5: Panels and reaction wheels revolute joints.

The same is done for the three reaction wheels, which provide the correct control torques acting on the CoM of the system.

### 3.1.3 Forces

In order to have more realistic hinges, simulating them as rotational spring-dampers, a kinematic study is done before. The analysis has been done about only one hinge, since results are the same for every joint.
A motion law (Fig. 3.6) is applied in order to investigate the torque applied by the motor to the respective hinge as function of the deployment angle of the same hinge.

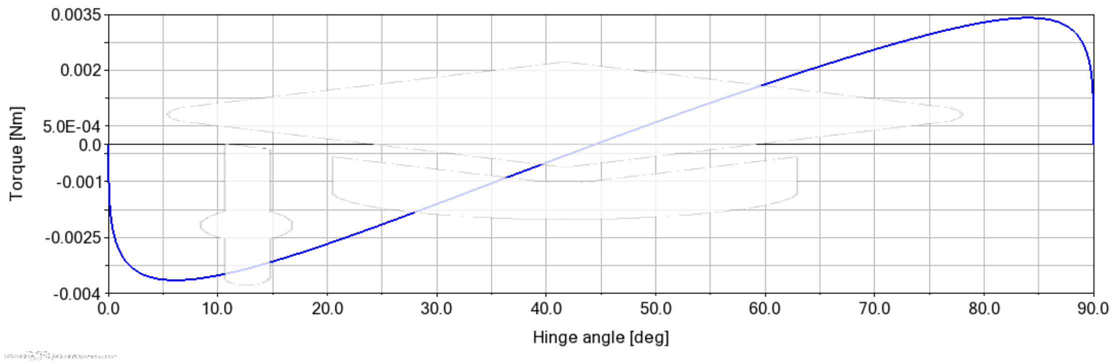


Figure 3.6: Torque between hinge panel and hub with a simple motion law.

A function STEP5 has been applied, taking the hinge angle from 0 to 90 deg in 60 s. From Fig. 3.6 it is evident that the spring-damper shall have a preload of $\approx 0.004$ $Nm$ and a torsional stiffness of $\approx 8 \cdot 10^{-5}$ $Nm/deg$, looking at peaks and slope of the curve. Finally, it has been decided to insert a null damping coefficient, going to complete the passage from a kinematic to a dynamic model.

After that a focus on the torque adapted to deploy the panel has been posed. It has been decided to use some functions already implemented in MSC Adams, in order to model braking and stopping of the panel motor. The following functions are used:

- IF(function to be evaluated: value if the function is $< 0$, value if the function is equal to 0, value if the function is $> 0$)

As function, the relative angular velocity of the hinge between panel and hub is chosen and depending on the positive rotational direction of the hinge, a value equal to the multiplication of a braking coefficient (value $< 0$) by the relative angular velocity is put into the field referring to the function $<$ or $> 0$.

- STEP(independent variable, a real variable that specifies the x value at which the STEP function begins, the initial value of the step, a real variable that specifies the x value at which the STEP function ends, the final value of the step) [23]

This function is useful to make the next function comes into play at the right moment. In particular, as independent variable, the deployment angle of hinge is chosen, setting a value equal to 0 at 89 deg and a value equal to 1 at 91 deg (for simplicity the positive case is presented, keeping in mind that in case of opposite positive rotation of the hinge values equal to 1 at -91 deg and 0 at -89 deg have to be chosen).

- BISTOP(the distance variable x you want to use to compute the force, the time derivative of x, the lower bound of x, the upper bound of x, a non-negative value that specifies the stiffness of the boundary surface interaction, a positive value that specifies the exponent of the force deformation characteristic, a non-negative variable that specifies the maximum damping coefficient, a positive real variable that specifies the penetration at which the full damping coefficient is applied)

The BISTOP function models a gap element. Fig. 3.7 illustrates the BISTOP force. The gap element consists of a slot which defines the domain of motion of a Part I located in the slot. As long as Part I is inside the slot and has no interference with the ends of the slot, it is free to move without forces acting on it. When Part I tries to move beyond the physical definition of the slot, impact forces representing contact are created by the BISTOP function. The created force tends to move Part I back into the slot.

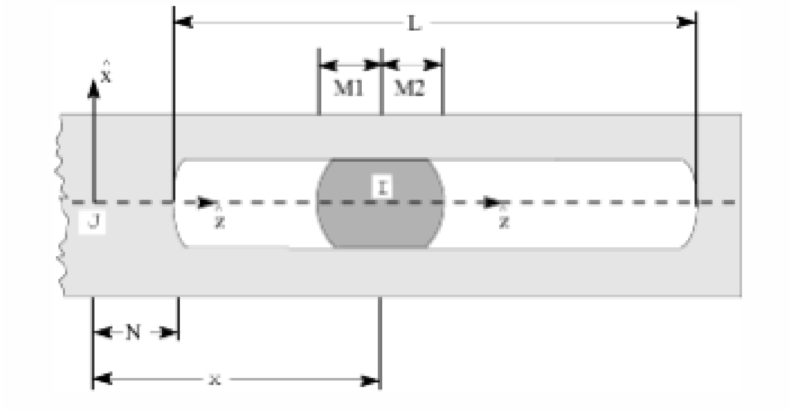


Figure 3.7: Bistop characterization.

The BISTOP force has two components: a stiffness component dependent on the penetration of Part I into the restricting Part J and a damping or viscous component that may be used to model energy loss [23].
In Fig. 3.8 the functions set for a positive rotating hinge are reported. As visible looking at the parameters chosen, it is clear that a value of deployment angle equal exactly to 90 deg is not immediately obtained. It has been decided to fix a range of two degrees (89-91 deg), in which BISTOP function (i.e. the stopping phase) plays its roll. If a more narrow range would have been selected, there would have been more stresses on the hinge.
In Fig. 3.9, 3.10 and 3.11 a comparison between two angle ranges is done. With the range selected there is a reduction of the force acting on the hinge of almost 0.1 N with a final angle difference of less than 0.9 deg and no significant variation for the angular velocity.

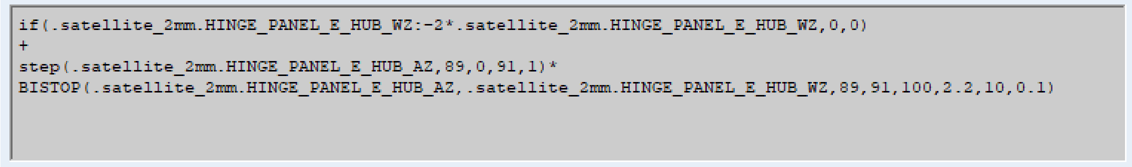


Figure 3.8: Hinge torque function.

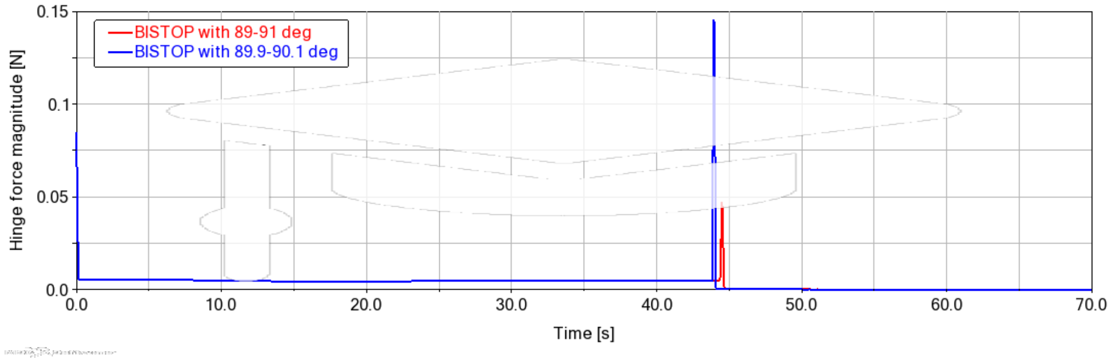


Figure 3.9: Hinge force.

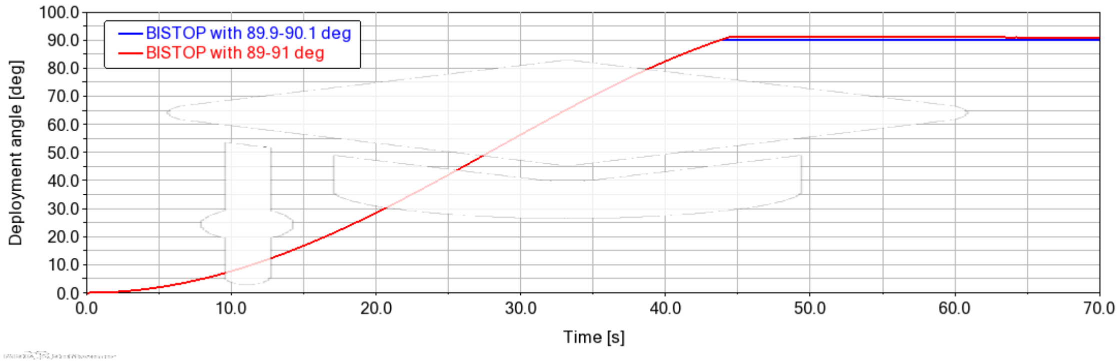


Figure 3.10: Panel deployment angle.

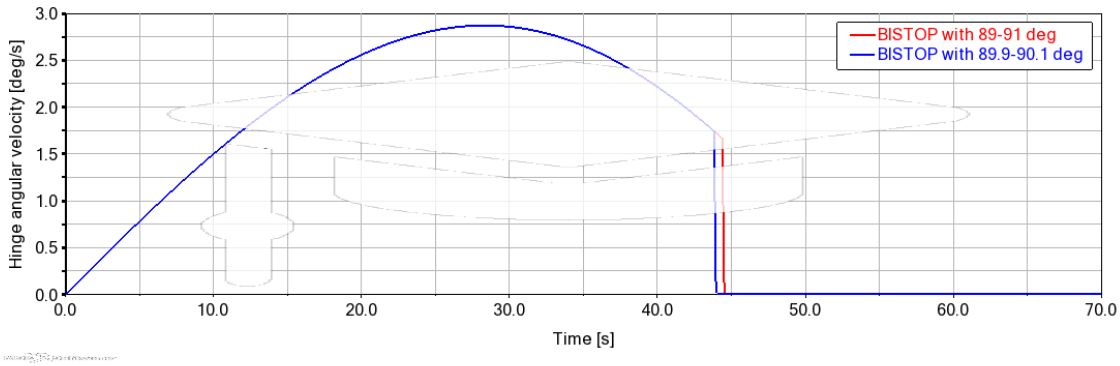


Figure 3.11: Panel deployment angular velocity.

## 3.2 Attitude control implementation

In this section it is presented how MSC Adams is put into communication with MATLAB/Simulink in order to control the attitude of the spacecraft during a manoeuvre that will be shown in the next chapter.
As previously said, it has been decided to operate the attitude control through a set of three reaction wheels located at the CoM of the system, acting along the three body axes and linked to the structure with three revolute joints (refer to Fig. 2.3, 3.3 and 3.5).
MSC Adams has the potential to create a Simulink block able to contain all system informations (plant); then, the user chooses which inputs and which output will be passed from and to that block. In this case of study nine state variable are created, three as inputs and six as outputs.

### 3.2.1 Inputs

As inputs to the Simulink block that will be generated by the software, it has been decided to pass the three reaction wheels torques, which will impress opposite torques to the spacecraft through the principle of action-reaction. To make this, three state variables equal to zero are created (Fig. 3.12) and passed as values to previously created torques acting on each wheel. The function VARVAL is used and will pass the values of the torques generated by every Simulink step of calculation (Fig. 3.13).

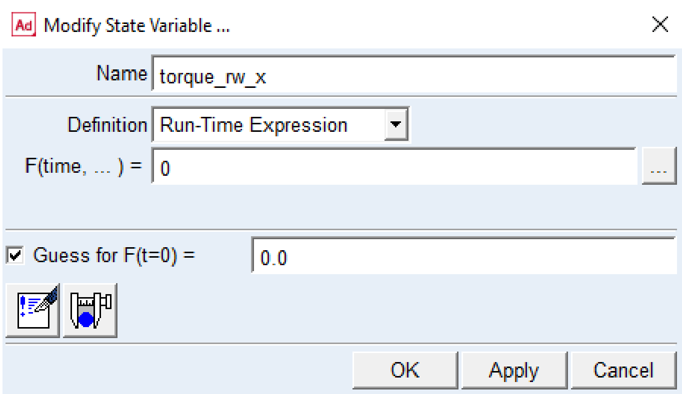


Figure 3.12: State variable creation (x-axis example).

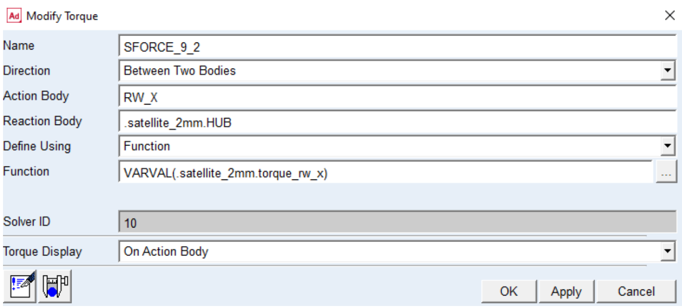


Figure 3.13: Reaction wheel torque definition (x-axis example).

Finally, the three state variables are passed to the command "create an Adams plant input".

### 3.2.2 Outputs

As outputs it has been decided to create six state variables: three representing the attitude angles of the spacecraft (Fig. 3.14) and three defining the three angular velocities (Fig. 3.15). These values will be crucial for the implementation of the attitude control in MATLAB/Simulink, providing the state of the spacecraft at every Simulink cycle.

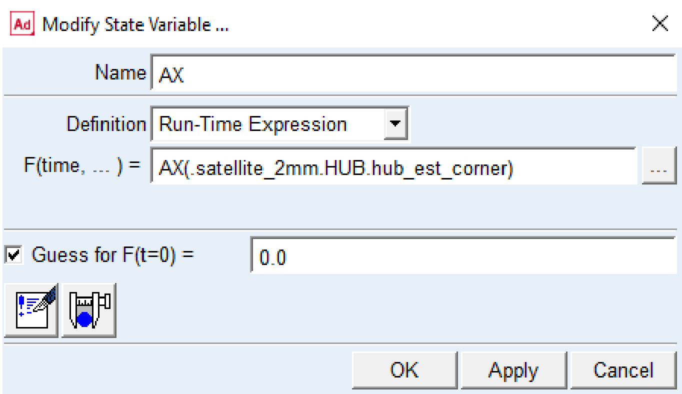


Figure 3.14: Roll angle state variable.

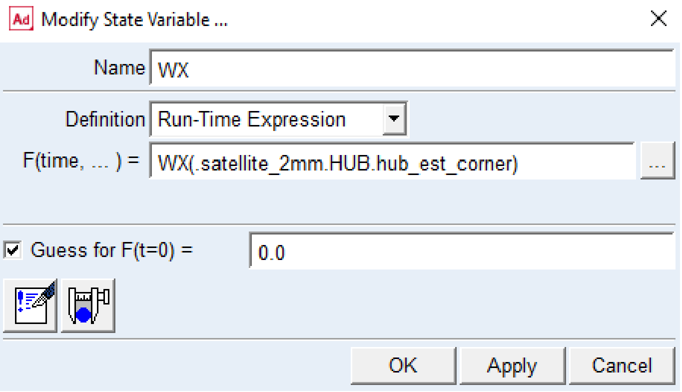


Figure 3.15: Roll angular velocity state variable.

Finally, the six state variables are passed to the command "create an Adams plant output".

# Chapter 4

# Simulation results

In this chapter the final comparison between the mathematical model for a flexible spacecraft and the multi-body non-linear analysis of the same spacecraft through MSC Adams is presented.
The chapter is organized as follows: in the first section the deployment of the solar panels in MSC Adams is analysed through a few considerations about hinge angles, deployment time and internal torques. In the following section a manoeuvre with an attitude controller studied in MATLAB/Simulink through the mathematical model is shown. What follows is a look to what happens in case of total rigid spacecraft, going to investigate the real influence of the flexible parts. After that, results of the simulation phases regarding the same manoeuvre obtained with MSC Adams are commented with respect to the previous ones. Finally, a case in which three of the four panels do not deploy themselves due to an on-board failure is assessed.

## 4.1 Solar panels deployment

Firstly, some results of a simulation for the deployment of the four flexible solar panels carried out in MSC Adams is presented.
In Tab. 4.1 some relevant data are reported (for the design implementation of the hinges refer to Chapter 3). It is important to remark that the final deployment angle will oscillate very slowly for the entire mission of the satellite in a range between 89 deg and 91 deg due to the parameters chosen for the stopping function (BISTOP) of each hinge.

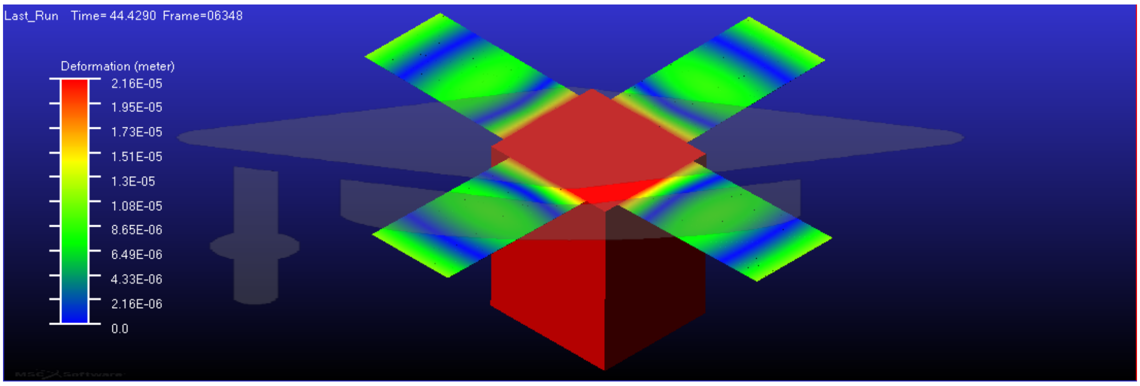


Figure 4.1: Deployment completed.

| | |
|---|---|
| Deployment time | ≈ 44.5 s |
| Deployment angle at deployment time | 91 deg |

Table 4.1: Deployment phase data.

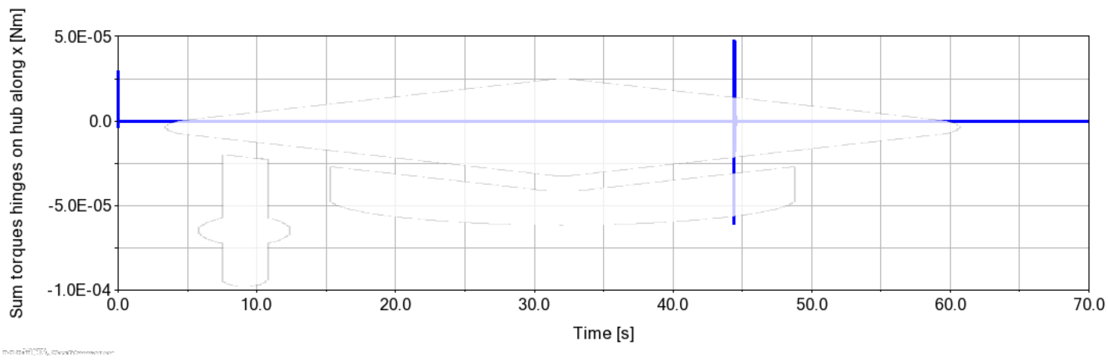


Figure 4.2: Sum of the torques generated by the deployment of the four hinges along x direction.

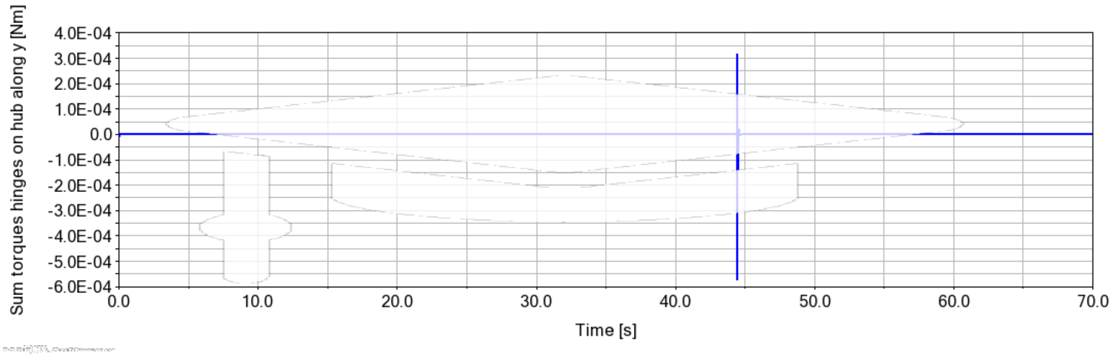


Figure 4.3: Sum of the torques generated by the deployment of the four hinges along y direction.

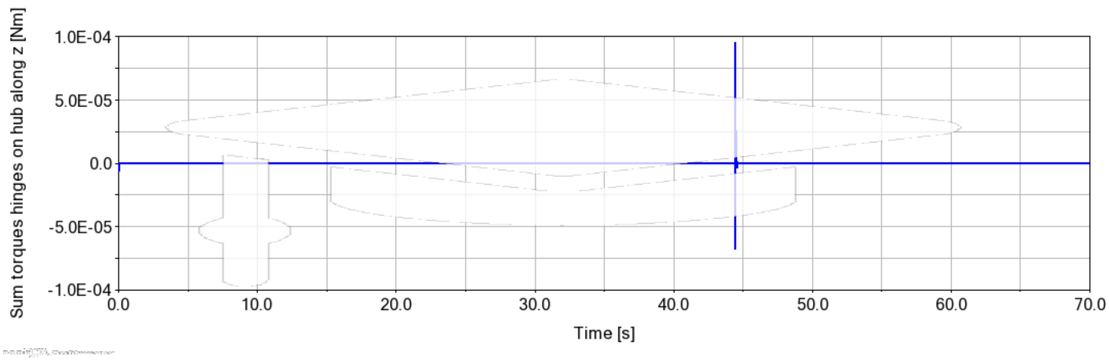


Figure 4.4: Sum of the torques generated by the deployment of the four hinges along z direction.

Due to the symmetry of the spacecraft, in Fig. 4.2, 4.3 and 4.4 it is shown that all the forces of the four hinges acting on the central main body generate a total torque close to zero along all the three body axes, fact that does not disturb highly the spacecraft attitude.

## 4.2 Manoeuvre with the mathematical model

For the flexible solar panels dynamics, a FEM analysis is performed in order to evaluate the natural frequencies, the mode shapes and the eigenvectors matrix used in the model. The FEM analysis is conducted with MSC Patran/MSC Nastran software. The four solar panels are modelled in MSC Patran as aluminium plates, and a modal analysis is performed. After that, the frequencies and eigenvectors obtained from the analysis are used in the simulation. A code is written in MATLAB to evaluate all the matrices in the dynamics equation of the flexible part, and the $\boldsymbol{\delta}$

coupling matrices defined in Chapter 2 are computed.
This section is divided in three parts: firstly, the FEM analysis results are reported; then, the simulation results are discussed; finally, a comparison with the case of rigid solar panels is assessed.

### 4.2.1 FEM analysis results

The results obtained from the FEM analysis in terms of frequencies and normal modes for each solar panel are shown in Tab. 4.2 and Fig. 4.5, 4.6 and 4.7. The first three normal modes have been evaluated with the modal analysis in MSC Patran/MSC Nastran: the first and third are bending modes, while the second one is a torsional mode. For the computation of the coupling matrices $\boldsymbol{\delta}_i$, for $i = 1, ..., 4$, these three modes have been taken into account.

Table 4.2: Natural frequency and damping of the three modes taken into account

| | Natural frequency [rad/s] | Damping |
|---|---|---|
| Mode 1 | 8.8850 | 0.0089 |
| Mode 2 | 34.5359 | 0.0345 |
| Mode 3 | 55.0985 | 0.0551 |

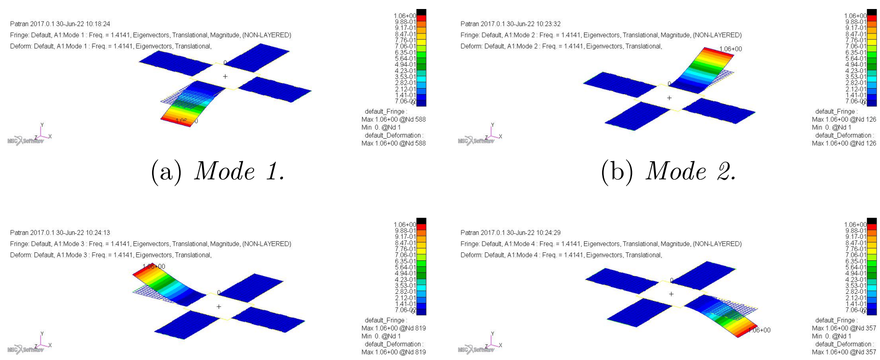

(a) *Mode 1.* (b) *Mode 2.*

(c) *Mode 3.* (d) *Mode 4.*

Figure 4.5: First bending mode.

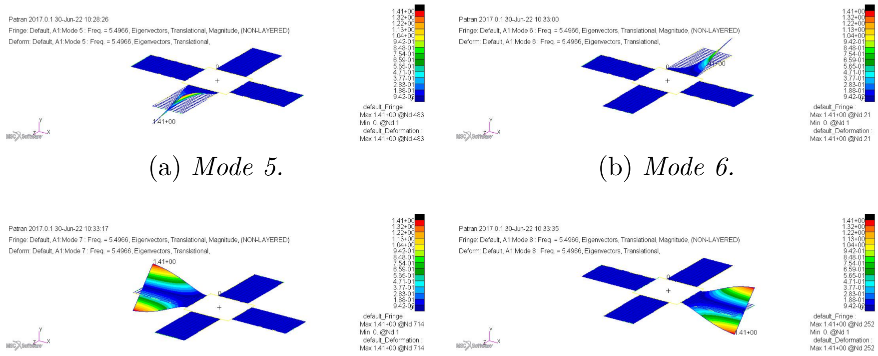

(a) *Mode 5.* (b) *Mode 6.*

(c) *Mode 7.* (d) *Mode 8.*

Figure 4.6: First torsional mode.

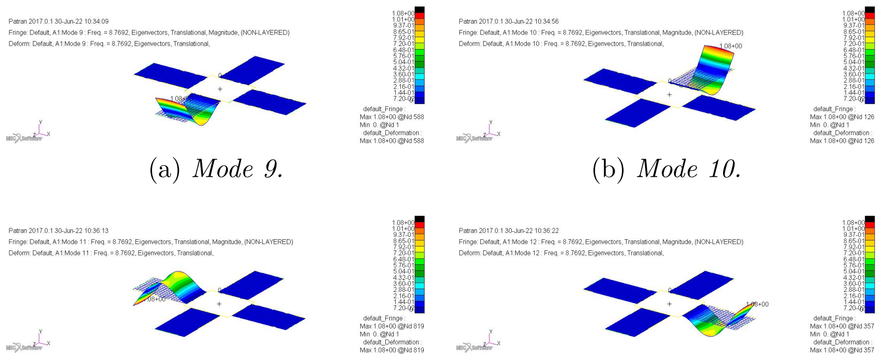

(a) *Mode 9.* (b) *Mode 10.*

(c) *Mode 11.* (d) *Mode 12.*

Figure 4.7: Second bending mode.

The values of natural frequencies in Tab. 4.2 are used to compute the stiffness matrix $\boldsymbol{K}$ and the damping matrix $\boldsymbol{C}$, for $\gamma = 0.002$. Knowing the damping matrix, the damping values in Tab. 4.2 can be obtained.
From the modal analysis, the eigenvectors for the sub-panels of each solar panel are evaluated. Hence, the four $N \times 3$ coupling matrices between the rigid hub and the flexible solar panels are obtained, with $N = 3$, equal to the number of shape modes:

$$\boldsymbol{\delta}_1 = \begin{bmatrix} -0.0121 & 0 & 1.7316 \\ -0.2253 & 0 & -0.1359 \\ 0.0093 & 0 & 1.0037 \end{bmatrix} \sqrt{Kg/m^2}$$

$$\boldsymbol{\delta}_2 = \begin{bmatrix} -1.6603 & 0 & -0.0525 \\ 0.0312 & 0 & -0.2253 \\ -0.9452 & 0 & 0.0403 \end{bmatrix} \sqrt{Kg/m^2}$$

$$\boldsymbol{\delta}_3 = \begin{bmatrix} -0.0121 & 0 & 1.7316 \\ -0.2253 & 0 & -0.1359 \\ 0.0093 & 0 & 1.0037 \end{bmatrix} \sqrt{Kg}/m^2$$

$$\boldsymbol{\delta}_4 = \begin{bmatrix} -1.6603 & 0 & -0.0525 \\ 0.0312 & 0 & -0.2253 \\ 0.9452 & 0 & -0.0403 \end{bmatrix} \sqrt{Kg}/m^2$$

### 4.2.2 Flexible spacecraft attitude manoeuvre

In order to test the effective influence of the flexibility of the solar panels on the spacecraft attitude, a manoeuvre of attitude changing is performed. The manoeuvre is carried out in MATLAB/Simulink environment, with a fixed sample time of 0.001 s, and the differential equations are solved with the ode4 (Runge-Kutta) solver.
In Fig. 4.8 the block scheme in Simulink is presented. There are five main subsystems:

- The most complex subsystem is the attitude kinematics and dynamics subsystem. It includes the spacecraft attitude kinematics and dynamics, through quaternions, Euler angles and Euler equations. This subsystem receives in input internal and external disturbances due to the flexibility of the solar panels and the influence of the environment (only the gravity gradient is considered), and the actuators torques, while it gives as output the Euler angles and the angular velocities necessary for the state feedback of the controller, and the angular accelerations for the dynamics of the solar panels.

- The PD controller subsystem receives in input the three Euler angles and the three angular velocities and provides the control torques. In particular, the PD gains are set as in Tab. 4.3:

| | |
|---|---|
| $K_P$ | 0.1 |
| $K_D$ | 2 |

Table 4.3: PD controller gains.

- The reaction wheels subsystem receives in input the control torques provided by the controller and gives as output the three reaction wheel torques and angular momentums (refer to Chapter 2 and Fig. 2.2).

- The solar panels subsystem contains the flexible dynamics model of the four panels. It receives in input the angular body accelerations and provides the solar panels torques and angular momentums.

- The gravity gradient subsystem represents the contribution of the external disturbances as example. It receives in input the Euler angles regarding roll and pitch and provides the gravity gradient torques.

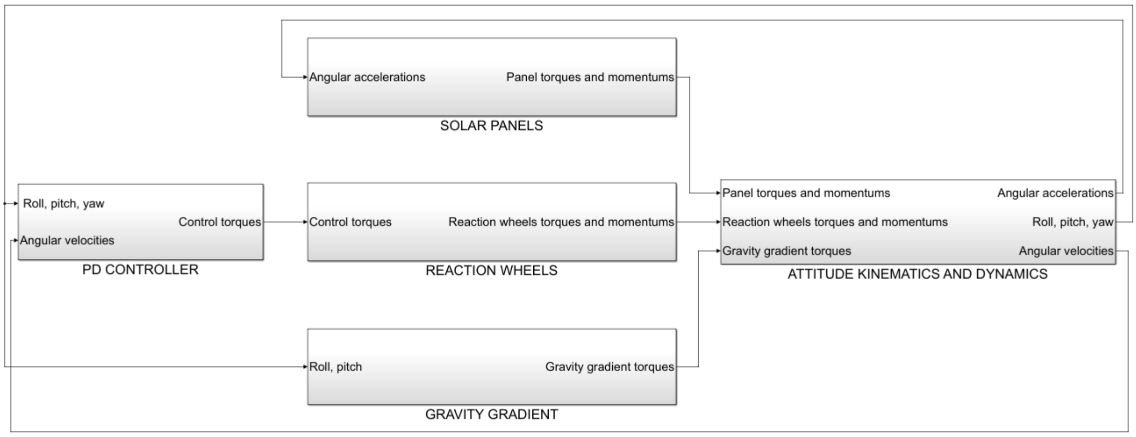


Figure 4.8: Flexible model simulink scheme.

The first mission scenario consists of a manoeuvre of attitude changing aiming at simulating a command for a new pointing direction for the satellite. The spacecraft starts the manoeuvre having already deployed its solar panels. Initially, the attitude is represented by the null quaternion $\boldsymbol{q}_0 = [1{,}0{,}0{,}0]^T$ and the goal of the manoeuvre is to reach the Euler angular position $[15{,}5{,}10]^T$ deg. Finally, at 500 s the spacecraft begins to restore its initial orientation, so $[0{,}0{,}0]^T$ deg. The simulation stops at 1000 s.
From Fig. 4.9 to Fig. 4.15 and in Tab. 4.4 the most relevant graphics and measures are reported. It is not superfluous to mention that the rise time has been calculated as the difference between the time at which the signal reaches 0.9 $y_{ss}$ and the time to reach 0.1 $y_{ss}$, where $y_{ss}$ means the attitude angular value the spacecraft has to reach.

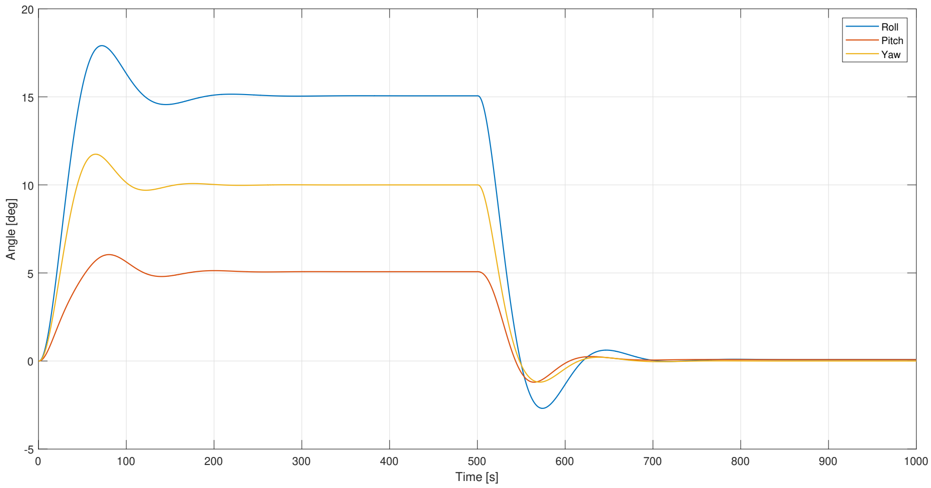


Figure 4.9: Flexible model angles.

Table 4.4: Flexible model control results.

| | Rise time [s] | Overshoot to reach $[15{,}5{,}10]^T$ deg [deg] | Angle at 500 s [deg] | Angle at 1000 s [deg] |
|---|---|---|---|---|
| Roll | 31.51 | 17.91 (19.4 %) | 15.06 | 0.08 |
| Pitch | 37.40 | 6.04 (20.8 %) | 5.07 | 0.08 |
| Yaw | 29.30 | 11.74 (17.4 %) | 10.00 | $-5.29 \cdot 10^{-5}$ |

As visible in Fig. 4.9 and Tab. 4.4, the signals have very few oscillations, due to the not so high effectiveness and quickness of the controller at damping and deleting the influence of the environment disturbance and the vibrations of the panels. Also at the end of the simulation a small but acceptable steady state error lasts.

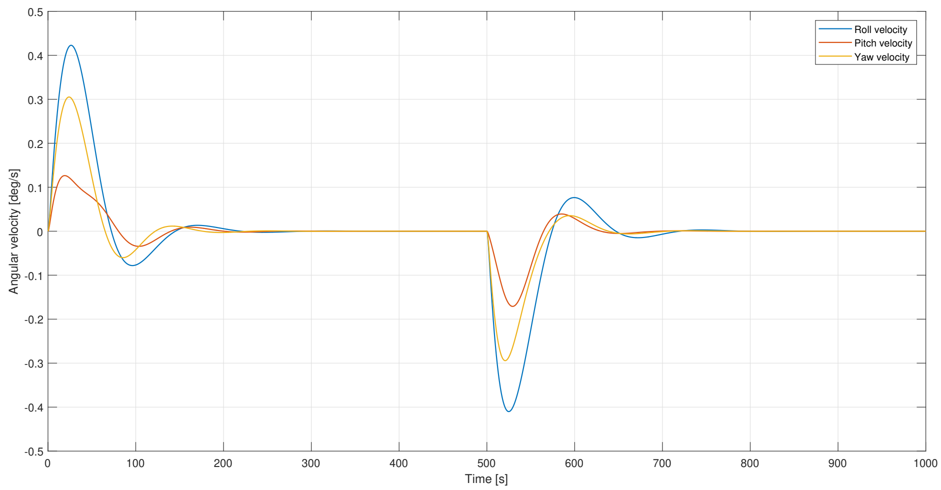


Figure 4.10: Flexible model angular velocities.

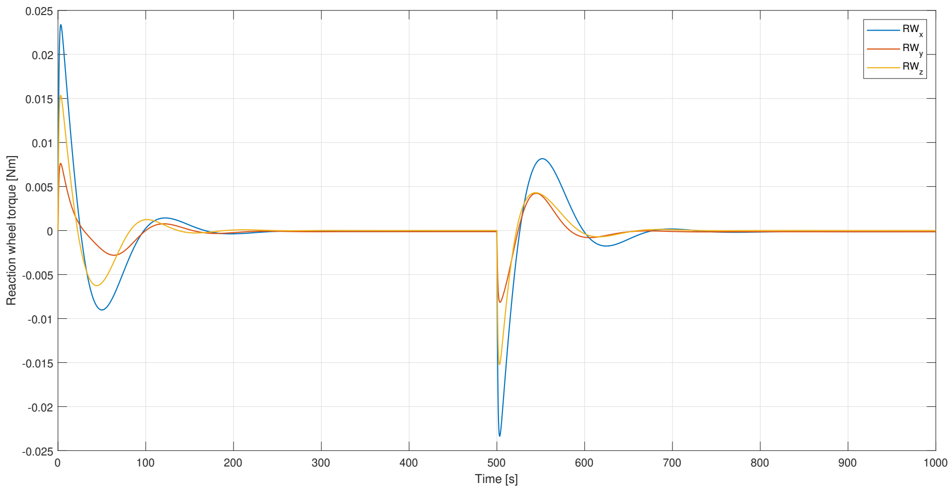


Figure 4.11: Flexible model reaction wheels torques.

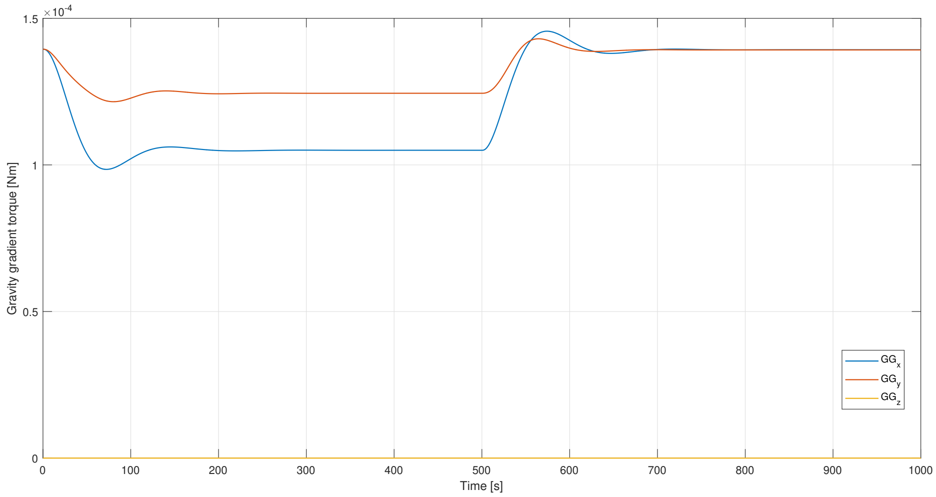


Figure 4.12: Flexible model gravity gradient torques.

Regarding angular velocities, satisfying values of $10^{-4}$ $deg/s$ at the end of the simulation are obtained. The actuators take action mainly during the input command for the manoeuvres, leaving small torques at the end aiming at counteracting disturbances and vibrations of the panels.

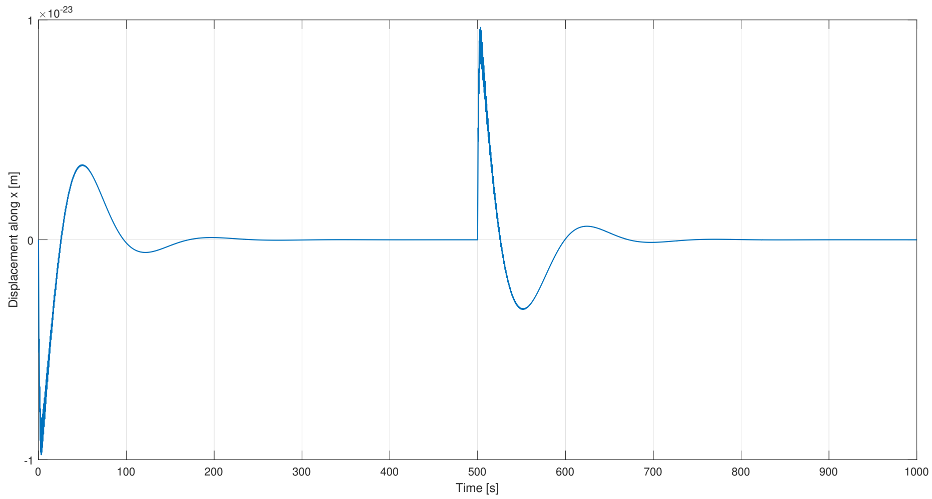


Figure 4.13: Flexible model deformation along x direction.

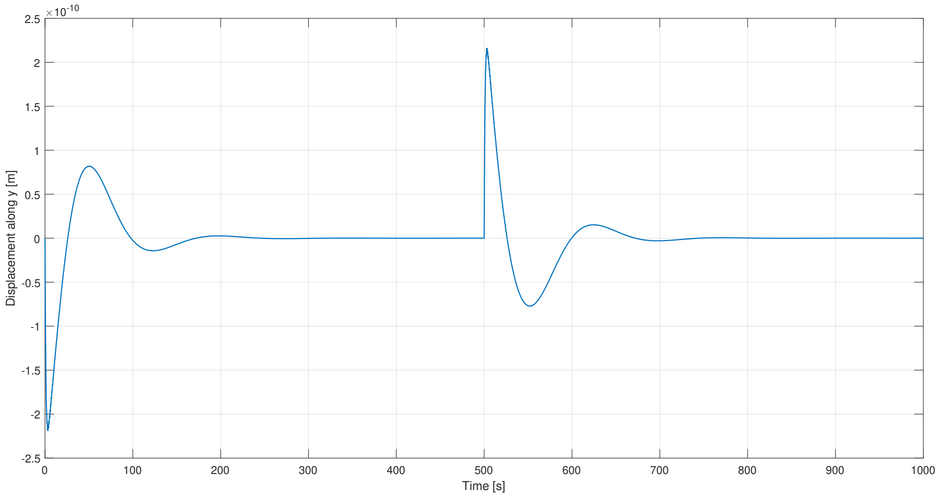


Figure 4.14: Flexible model deformation along y direction.

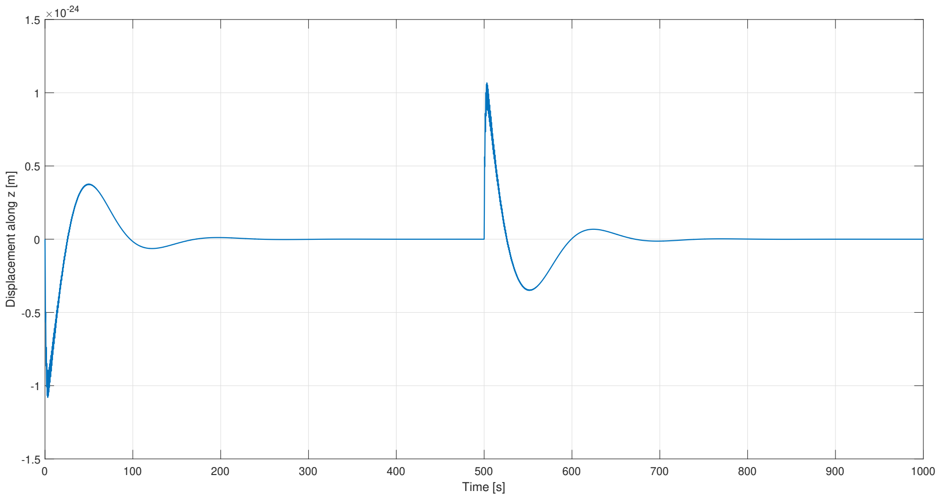


Figure 4.15: Flexible model deformation along z direction.

There are very low deformations of the panels due to the approximated implementation exploiting the linear FEM analysis in MSC Patran/MSC Nastran. For the reference system, refer to Fig. 2.10.

### 4.2.3 Rigid spacecraft comparison

It is reported here the case of total rigid spacecraft, in order to comment the influence of the flexibility of the solar panels shown before. The solar panels subsystem representing the solar panels dynamics disappears. The spacecraft is treated as only one body including the solar panels, going to variate the total inertia matrix, the dimensions and the global weight.

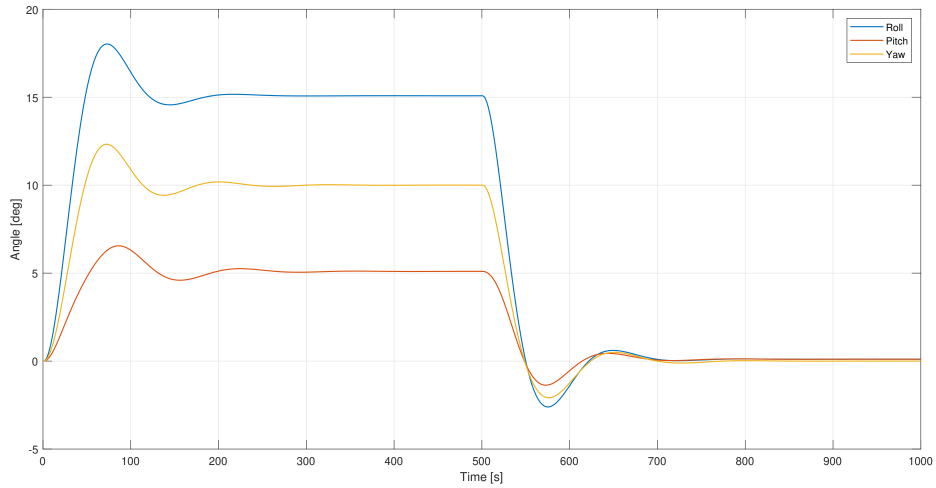


Figure 4.16: Rigid model angles.

Table 4.5: Rigid model control results.

| | Rise time [s] | Overshoot to reach $[15,5,10]^T$ deg [deg] | Angle at 500 s [deg] | Angle at 1000 s [deg] |
|---|---|---|---|---|
| Roll | 31.85 | 18.03 (20.2 %) | 15.08 | 0.11 |
| Pitch | 36.04 | 6.55 (31.0 %) | 5.10 | 0.11 |
| Yaw | 31.72 | 12.33 (23.3 %) | 10.00 | $1.41 \cdot 10^{-4}$ |

From Tab. 4.5 it is clear that only roll and pitch show small steady state errors, due to the influence of the gravity gradient on them. The roll and pitch errors at the end of the simulation result a little bit more than before because the gravity gradient is a little bit more than in the flexible model case.

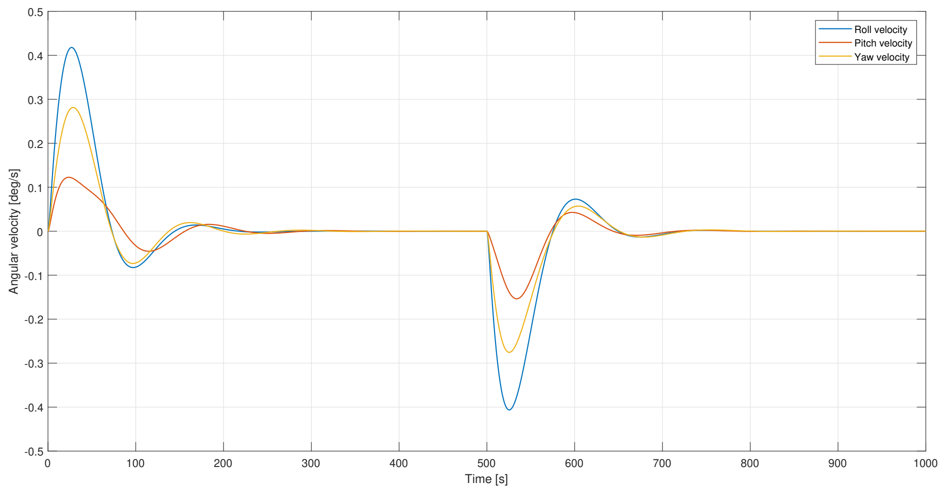


Figure 4.17: Rigid model angular velocities.

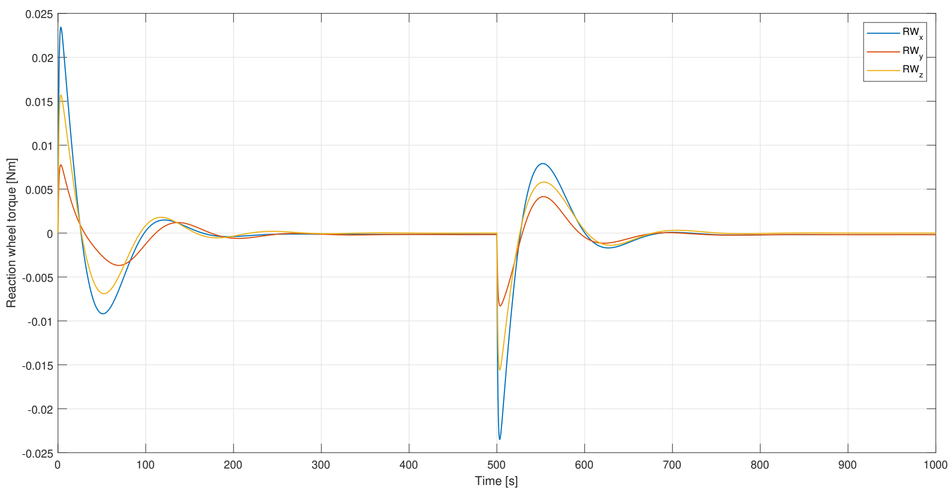


Figure 4.18: Rigid model reaction wheels torques.

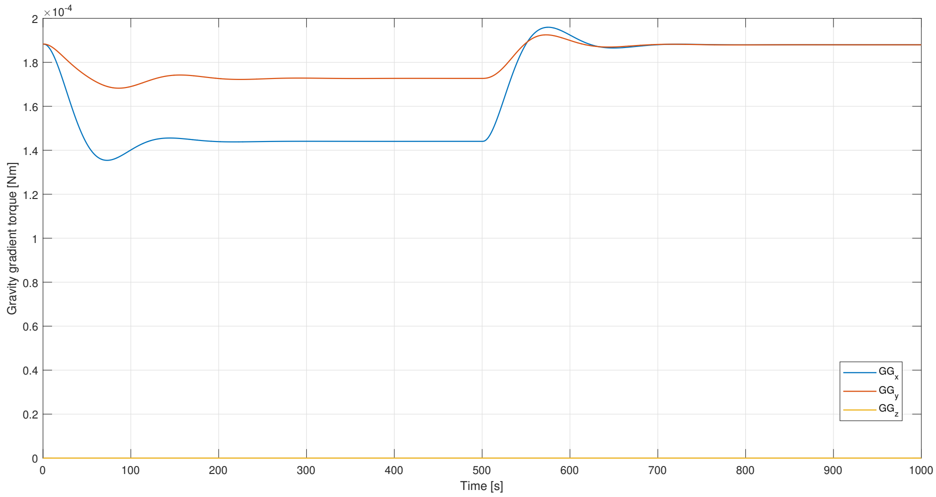


Figure 4.19: Flexible model gravity gradient torques.

At the end of the manoeuvre the angular velocities are very close to zero ($10^{-6}$ $rad/s$) and the reaction wheels provide torques of about $10^{-4}$ $Nm$ to hinder the gravity gradient action.
Since the solar panels used for the flexible mathematical model result very rigid, there are not so many differences between the flexible and the rigid model.

## 4.3 Manoeuvre in MSC Adams

In this section the same previous manoeuvre is analysed through the spacecraft implementation in MSC Adams environment. With respect to the mathematical model, in this case the whole content of the blocks regarding the attitude kinematics and dynamics and the solar panels is substituted by an unique big block exported from MSC Adams into Simulink (Fig. 4.20). This is possible thanks to the tool Adams Controls, that allows to connect a MSC Adams model to block diagram models developed with control applications such as Easy5 or MATLAB/Simulink, as already discussed during the introduction of this thesis. The new block, representing the entire plant, receives in input and provides in output what has been shown in the last section of Chapter 3. The manoeuvre is so carried out in MATLAB/Simulink environment, with a fixed sample time of 0.1 s and ode4 solver. The main parameter to be set was the Adams communication interval and 0.1 s has been chosen.

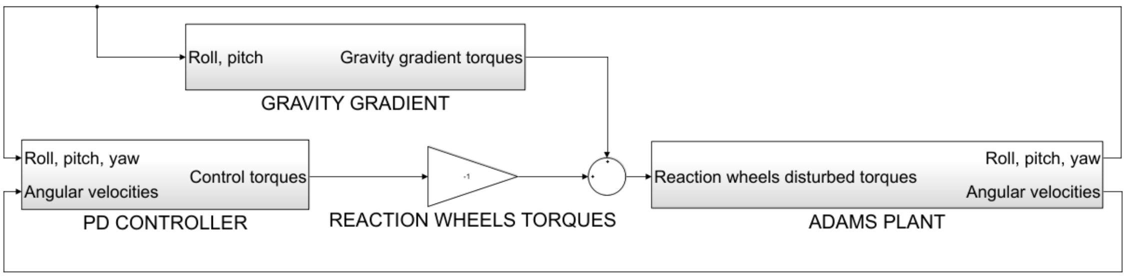


Figure 4.20: MSC Adams model simulink scheme.

It is relevant to say that in this case there are some differences with respect to the mathematical model simulation. At 0 s the spacecraft starts deploying the solar panels. Once the solar panels are deployed the manoeuvre can begin. So from the initial angular position defined by the null quaternion $\boldsymbol{q}_0 = [1,0,0,0]^T$, at 70 s the satellite begins to move to the Euler angular position $[15,5,10]^T$ deg. Finally, as during the previous case, at 500 s the spacecraft receives the command to go back to the initial angular position $[0,0,0]^T$ deg. Also this simulation stops at 1000 s. In Fig. 4.29 some steps of the simulation are shown.

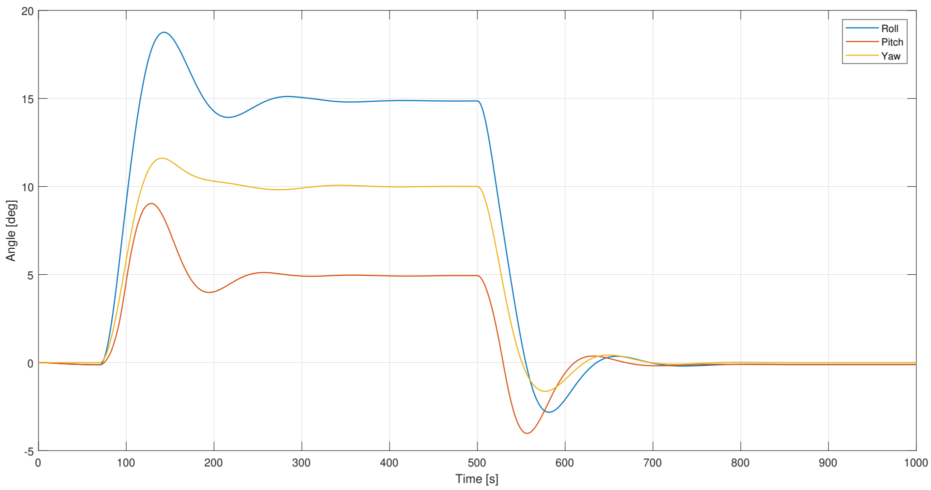


Figure 4.21: MSC Adams model angles.

Table 4.6: MSC Adams model control results.

| | Rise time [s] | Overshoot to reach $[15,5,10]^T$ deg [deg] | Angle at 70 s [deg] | Angle at 500 s [deg] | Angle at 1000 s [deg] |
|---|---|---|---|---|---|
| Roll | 30.85 | 18.76 (25.1 %) | -0.12 | 14.86 | -0.11 |
| Pitch | 18.95 | 9.04 (80.8 %) | -0.12 | 4.94 | -0.11 |
| Yaw | 31.90 | 11.61 (16.1 %) | $5.74 \cdot 10^{-5}$ | 10.00 | $8.75 \cdot 10^{-5}$ |

In Fig. 4.21 it can be observed that despite the high overshoots (especially for the pitch), the response is pretty stable and reaches good values at 500 s, even if the manoeuvre has less time to be carried out than before, because in the first phase the deployment of the solar panels occurs. Also here, at the end of the simulation there are small steady state errors caused mainly by the gravity gradient, since the deformations of the panels are close to zero, as reported from Fig. 4.24 to Fig. 4.28.

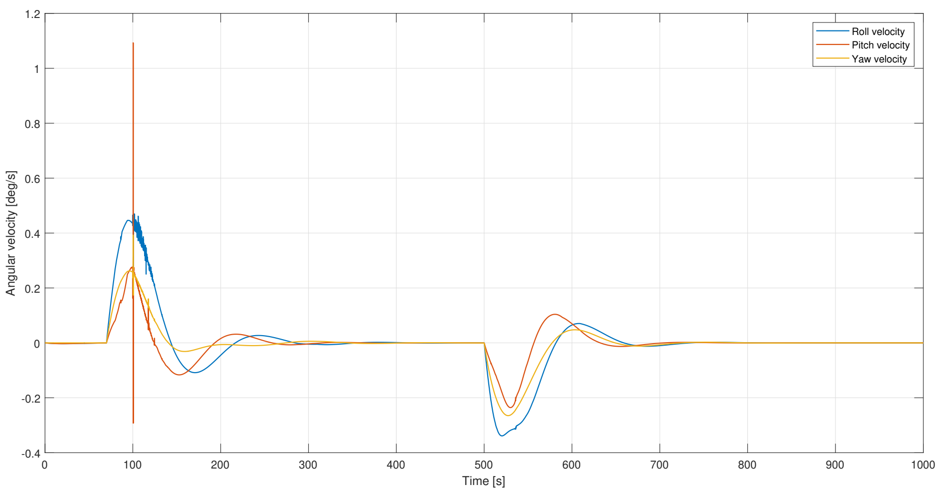


Figure 4.22: MSC Adams model angular velocities.

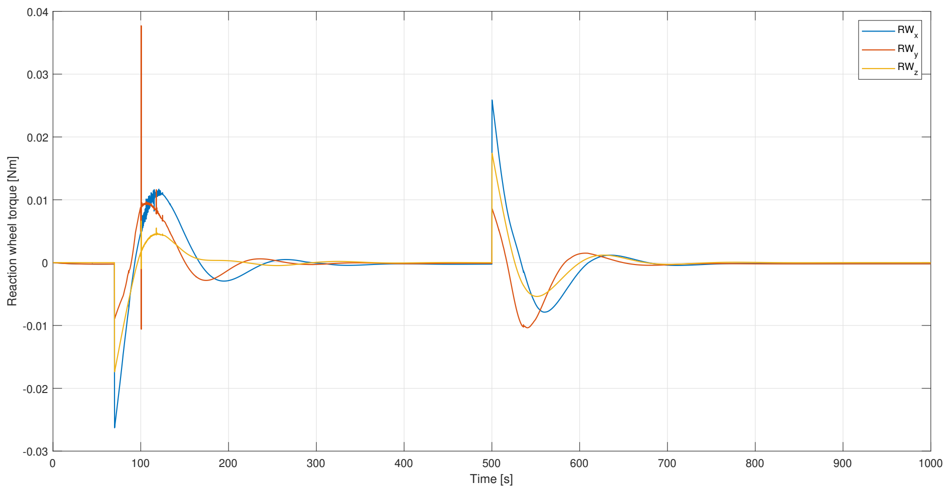


Figure 4.23: MSC Adams model reaction wheels torques.

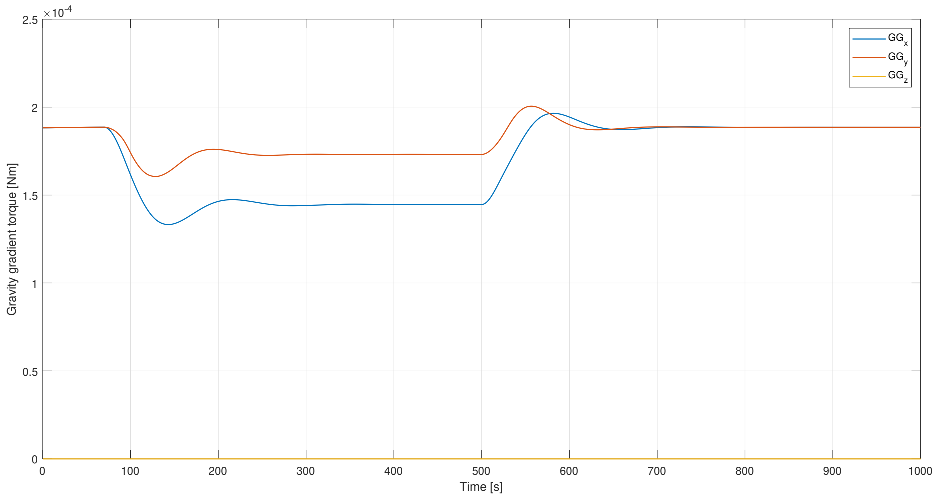


Figure 4.24: MSC Adams model gravity gradient torques.

As in evidence in Fig. 4.22 and Fig. 4.23, there are vibrations at about 100.4 s. The spacecraft has a big change of angular velocity and the reaction wheels react to counteract the effect. However there is a good response in terms of angular velocities because they reach $10^{-6}$ $deg/s$ at the end of the simulation. Regarding the reaction wheels there is almost the same behaviour, providing a final torque of $10^{-4}$ $Nm$ just on roll and pitch axes in order to counteract the gravity gradient.

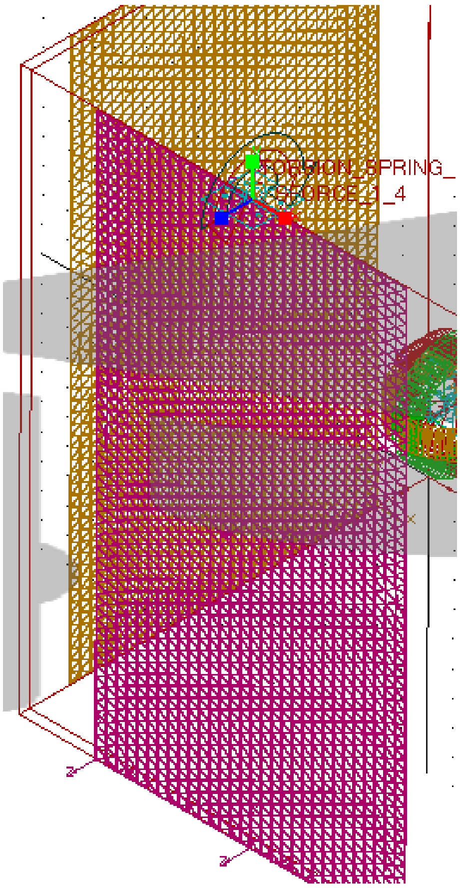


Figure 4.25: Deformations reference system.

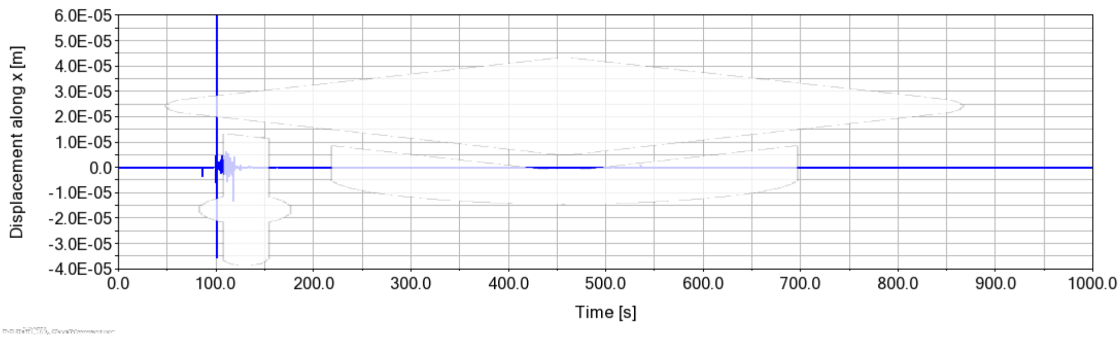


Figure 4.26: MSC Adams model deformation along x direction.

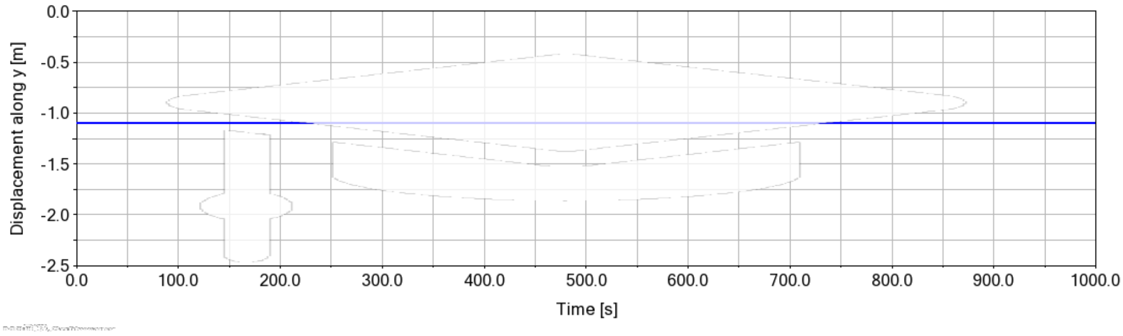


Figure 4.27: MSC Adams model deformation along y direction.

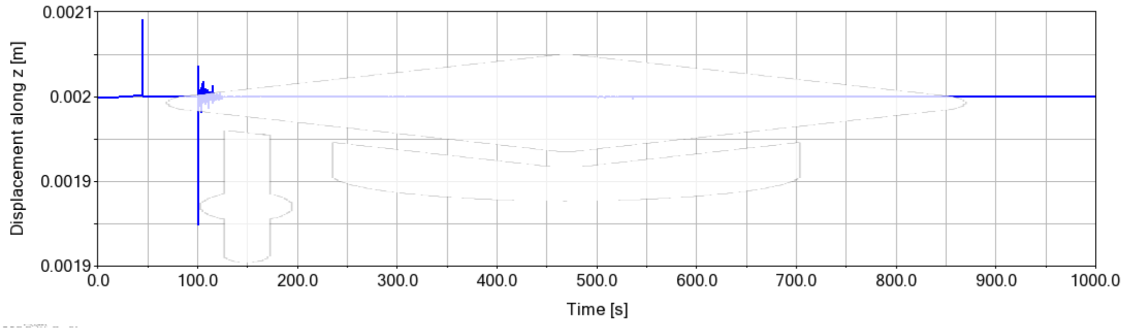


Figure 4.28: MSC Adams model deformation along z direction.

From Fig. 4.26 to Fig. 4.28 the translational displacements of a node at the tip of a panel with respect to the node fixed at the hinge are exposed. The marker representing the fixed node rotates with the hinge (x in red, y in green, z in blue, as visible in Fig. 4.25). There is not stretching or compression of the panel along y direction, while along x and z there are peaks at the stopping of the solar panels in deployed position and when the strong vibration at 100.4 s occurs. There is a big difference of values with respect to the mathematical model; this fact happens because it is very difficult to set the same values of damping ratios of the solar panels used for the previously discussed model. Not only, besides that it is necessary to consider that different meshes have been used (2D shell elements for the mathematical model and 3D tetrahedral elements for the MSC Adams model) and on one hand the panels are fixed to the central main body, by the other hand the panels are attached to the hub through a revolute joint, that is more realistic. Not only, as previously said, MSC Adams allows a non-linear study, so every kind of vibration is caused by the coupling among all the elements creating the system, thing that cannot be detect by a simple linear FEM analysis in MSC Patran/MSC Nastran.

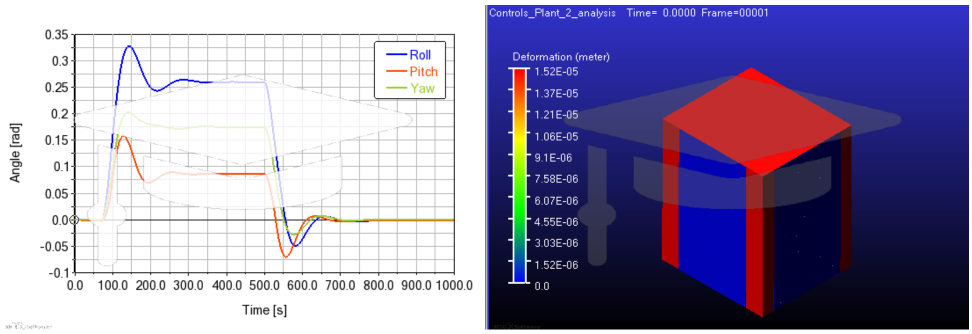


(a) *Time = 0 s.*

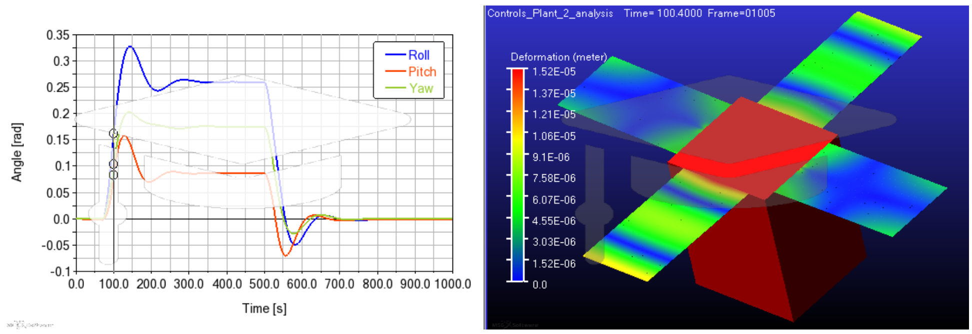


(b) *Time = 100.4 s.*

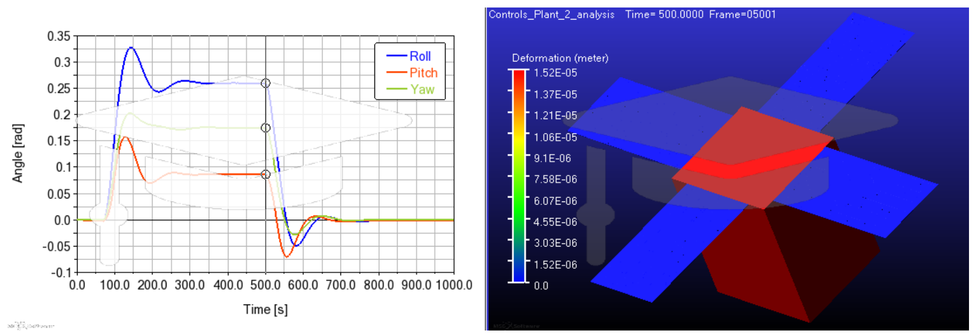


(c) *Time = 500 s.*

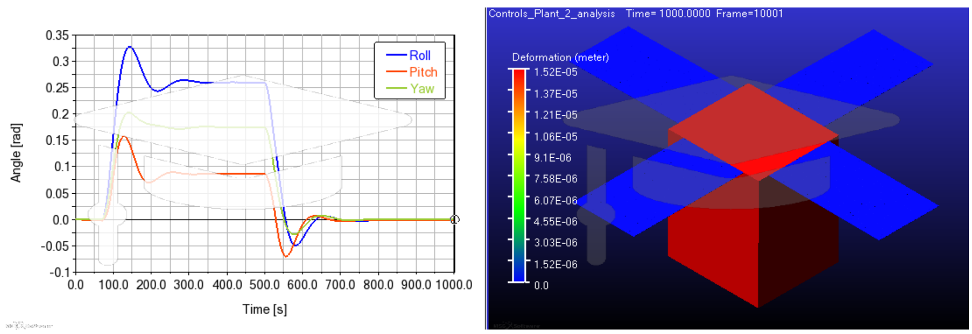


(d) *Time = 1000 s.*

Figure 4.29: Main simulation steps.

## 4.4 Failure of three solar panels

In this final section, it has been decided to test the PD controller during a failure. Only the deployment phase is discussed. The failure case is simulated through the deployment of just one panel, with the other three blocked in their initial position. The simulation is conducted as before in MATLAB/Simulink environment, exploiting the plant exportation from MSC Adams. The simulation settings are set with a fixed step time of 0.01 s and ode4 solver, and besides that 0.01 is set as Adams communication interval. The deployment command is given at the very beginning, at time 0 s, and the simulation stops at 300 s. In Fig. 4.38 some steps of the simulation are shown.

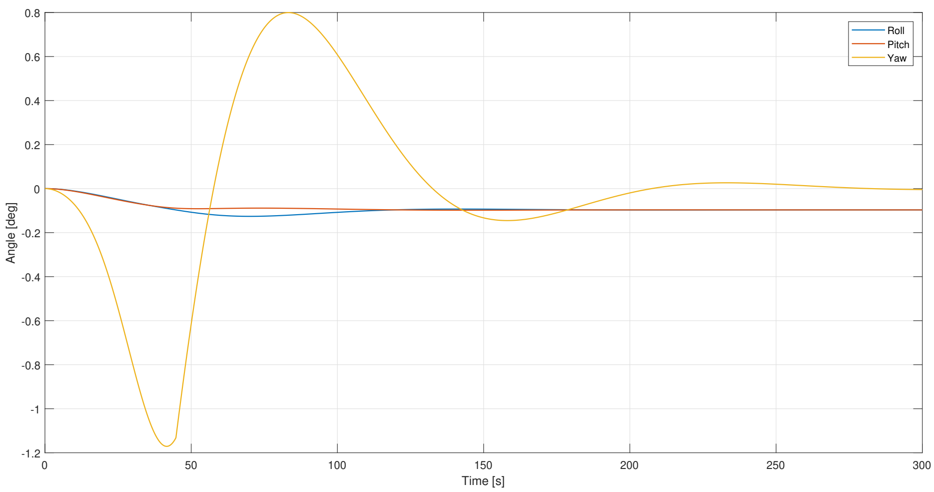


Figure 4.30: MSC Adams failure model angles.

In Fig. 4.30 it is visible that the biggest disturb is along z axis, due to the deployment of only one panel about that direction. The controller has a good response and takes back the yaw angle to zero. The other two angles, roll and pitch, are under the influence of the gravity gradient and, as already seen in the previous cases, a steady state error of -0.09 deg continues. So, although a manoeuvre does not occur, the controller does not manage to keep the spacecraft with the same initial pointing position, revealing a lack of effectiveness in case of on-board failure.

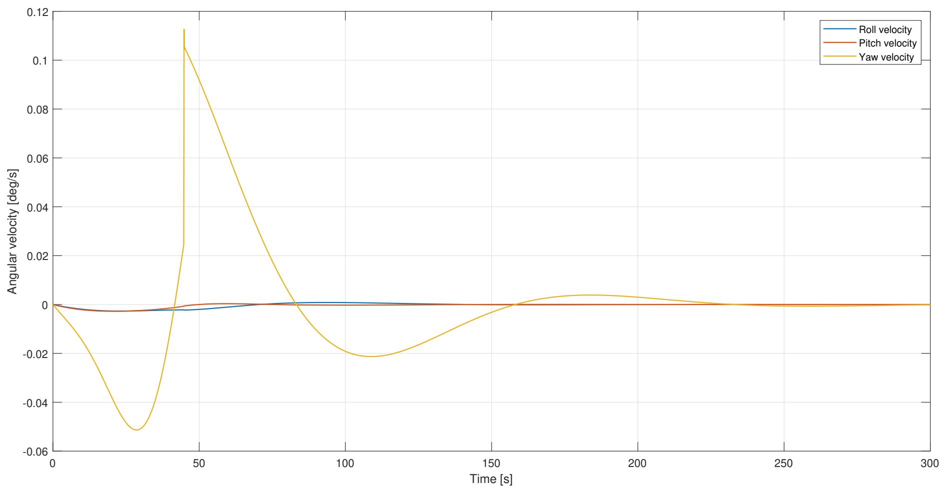


Figure 4.31: MSC Adams failure model angular velocities.

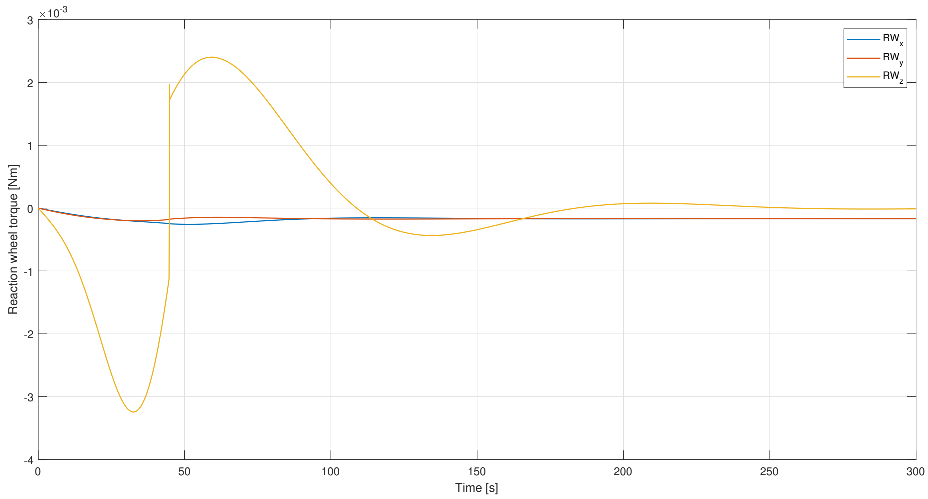


Figure 4.32: MSC Adams failure model reaction wheels torques.

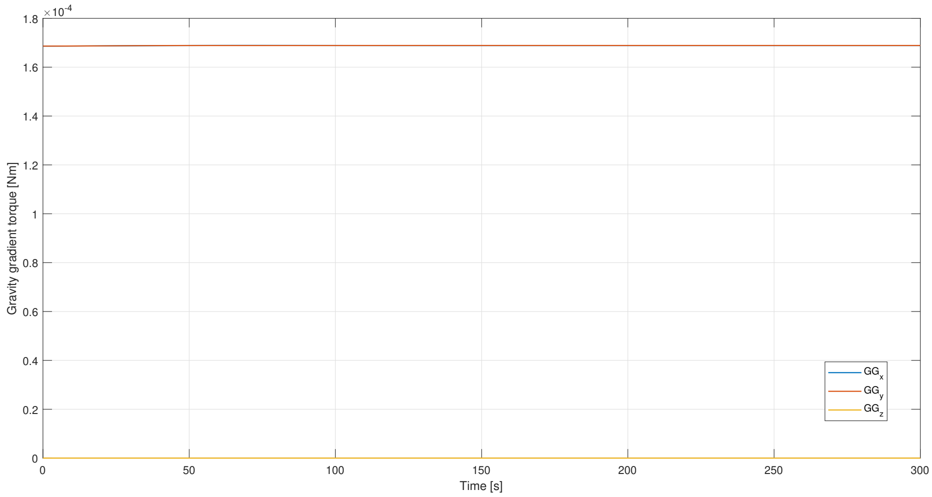


Figure 4.33: MSC Adams failure model gravity gradient torques.

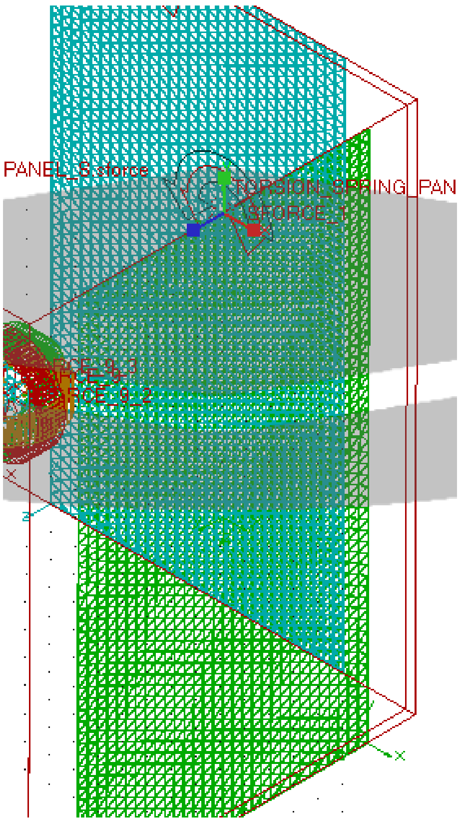


Figure 4.34: Deformations reference system.

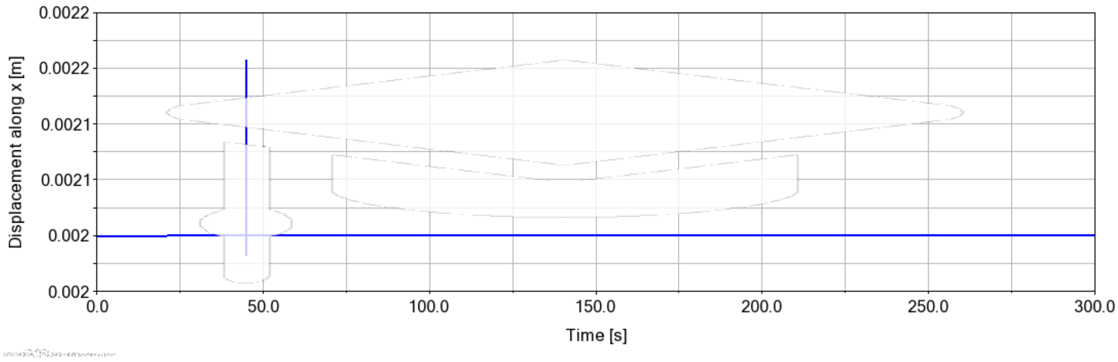


Figure 4.35: MSC Adams failure model deformation along x direction.

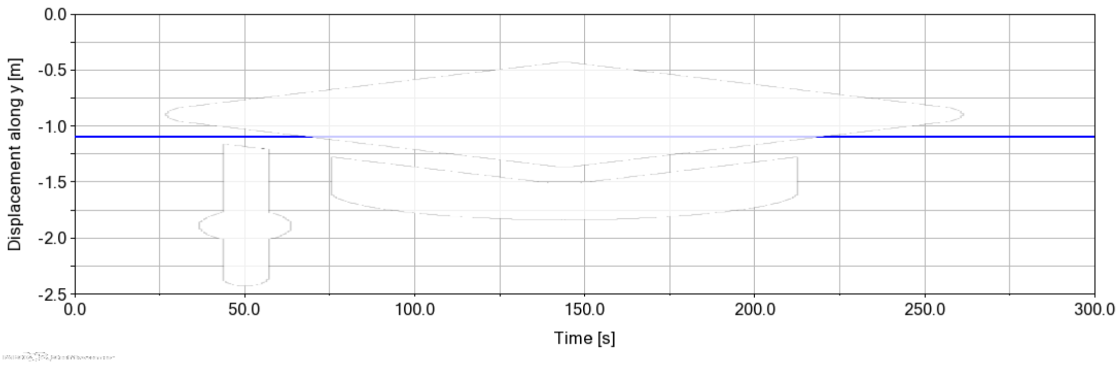


Figure 4.36: MSC Adams failure model deformation along y direction.

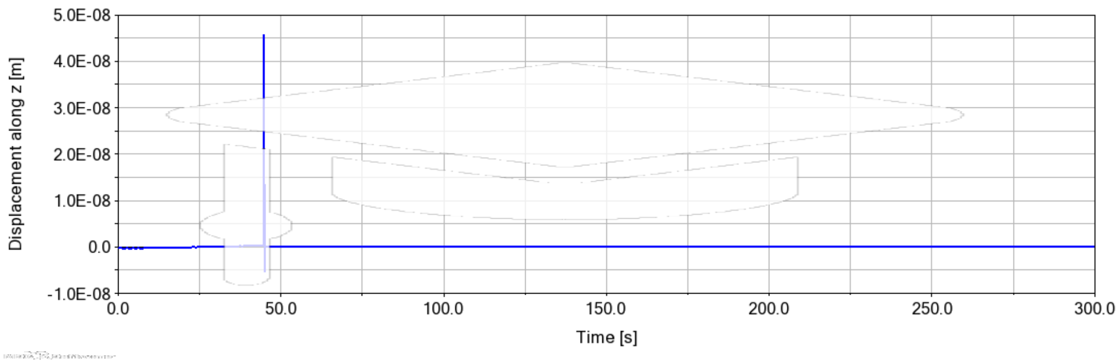


Figure 4.37: MSC Adams failure model deformation along z direction.

From Fig. 4.31 and 4.32 the strong influence of the stopping moment of the panel in deployed position is understandable. In fact, at approximately 44.8 s the angular

velocity increases quickly and the reaction wheels try to counteract that.
Regarding the deformations for a node at the tip of the deploying panel, the reference system is almost the same as in the previous section, with x in red, y in green and z in blue, and rotates fixed with the panel (Fig. 4.34). There are very low deformations along x and z direction, in particular at the stopping of the panel in deployed position, as it was expected (Fig. 4.35, 4.36 and 4.37).

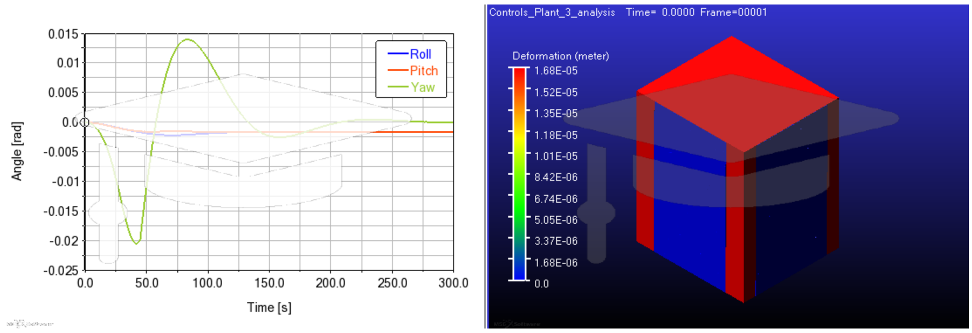


(a) *Time = 0 s.*

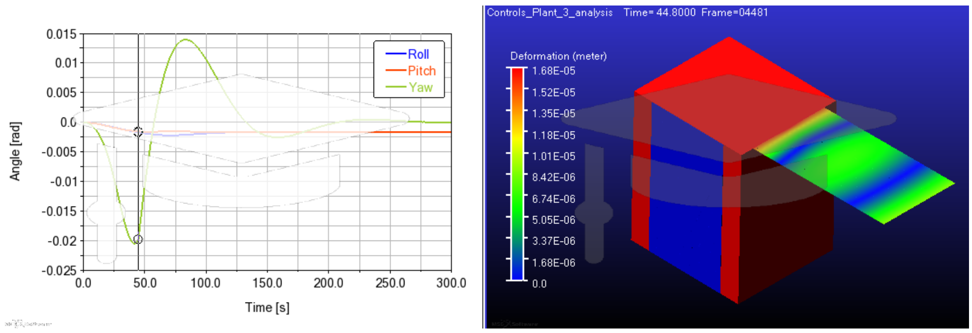


(b) *Time = 44.8 s.*

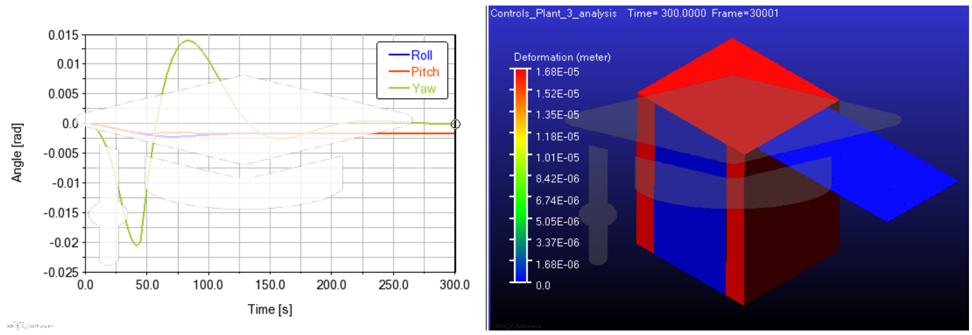


(c) *Time = 300 s.*

Figure 4.38: Main simulation steps.

# Chapter 5

# Conclusions and future works

This thesis aimed at validating the mathematical models to simulate the attitude dynamics of a flexible spacecraft, taking the Picard satellite as the main body of the spacecraft. Several tasks were addressed in this work. A mathematical model was derived for the satellite, by integrating the Euler equations with the solar panel flexibility equations as described in [2]. Besides that, a set of three reaction wheels was included as actuators. The flexible solar panels have been studied through a modal analysis with MSC Patran/MSC Nastran. The natural frequencies and eigenvectors obtained have been used for the implementation of the flexible panels' model in MATLAB/Simulink. In this thesis, the evaluation of the coupling matrix between the rigid hub and the flexible appendages was performed, together with the stiffness and damping matrices. Furthermore, the main task of this work was the development of a more realistic spacecraft in MSC Adams. This software was used to model the re-configurable satellite, taking into account the flexibility of the solar panels. Thanks to MSC Adams, it was possible to find many different results, like the response of the spacecraft to the control torques applied by the reaction wheels, in terms of attitude angles, angular velocities, stresses and the effect of the solar panels deployment, taking into account non-linearities. It was very difficult to create the same spacecraft used for the mathematical model, since it is tricky to set the same values of stiffness and damping ratios for the flexible solar panels. Not only, anyway the two spacecrafts were different due to the approximation with which one has been modeled and the complexity with which the other has been developed. So our final goal was to verify that, despite the simplicity and linearity of the mathematical model, it is a good approximation with which a user could study and analyse an attitude manoeuvre of a real spacecraft. In order to compare the two different models, the same PD controller was used to achieve the desired attitude angles. This automatic attitude control was applied to the mathematical model through

MATLAB/Simulink, and to the spacecraft developed in MSC Adams, linking the software to MATLAB through the sub-tool Adams Controls. The results obtained for the comparison are satisfactory, since there are very similar values for the response in both cases. The strong vibration at 100.4 s is not read by the mathematical model, revealing a little lack of accuracy. The PD controller ensures good performance in both cases, counteracting the influence of the environment disturbances and the vibrations of the flexible solar panels, but it has a lack of effectiveness during a case in which an on-board failure occurs, leaving the spacecraft to deviate of very few degrees the initial pointing orientation.
Possible future works are relative to the development of a more accurate model in MSC Adams, going to create even more realistic solar panels, with just the contour in aluminium, but with different, lighter materials inside, simulating solar cells. Moreover, the position dynamics and control can be implemented, together with the attitude dynamics, to have a complete model of the spacecraft. Besides that, a very simple cluster of reaction wheels has been created, so it could be improved with one reaction wheel more as redundancy, in a classic pyramidal configuration. Finally, a more effective controller can be used, in order to reduce the steady state errors and to avoid the not so negligible overshoots obtained during the manoeuvres.

# Bibliography


[1] Elisa Capello Pierangela Morga Mauro Mancini. "Flexible Spacecraft Model and Robust Control Techniques for Attitude Maneuvers". In: (2022).

[2] P. W. Likins. "Dynamics and Control of Flexible Space Vehicles". In: Edizione 32,Parte 1329 di JPL technical report NASA contractor report. 1970.

[3] Pierangela Morga. "Flexible Spacecraft Modelling and Control with a Robotic Manipulator". MA thesis. Politecnico di Torino, Apr. 2021.

[4] Herbert J. Kramer. *Picard*. https://directory.eoportal.org/web/eoportal/satellite-missions/p/picard. eoPortal Directory. 2022.

[5] *Picard*. https://en.wikipedia.org/wiki/Picard_(satellite). Wikipedia.

[6] *Adams: The Multibody Dynamics Simulation Solution*. https://www.mscsoftware.com/en-uk/product/adams. Hexagon.

[7] James B McConville and Joseph F McGrath. "Introduction to ADAMS theory". In: *Ann Arbor (MI): Mechanical Dynamic Inc* (1997).

[8] Daniele Catelani. *ADAMS/Flex*. Dispense del corso di Strutture per Veicoli Spaziali. Politecnico di Torino, 2019/20.

[9] F. Landis Markley and John L. Crassidis. "Attitude Kinematics and Dynamics". In: *Fundamentals of Spacecraft Attitude Determination and Control*. New York, NY: Springer New York, 2014, pp. 67–122. ISBN: 978-1-4939-0802-8. DOI: 10.1007/978-1-4939-0802-8_3. URL: https://doi.org/10.1007/978-1-4939-0802-8_3.

[10] Giulio Avanzini. "Dispense del Corso di Dinamica e Controllo di Assetto di Satelliti". In: *Spacecraft Attitude Dynamics and Control*. Ver. 3.0.0. 2008-09.

[11] Alam Mashiul et al. "Analytical and Experimental Study Using Output-Only Modal Testing for On-Orbit Satellite Appendages". In: *Advances in Acoustics and Vibration* 2009 (Apr. 2009). DOI: 10.1155/2009/538731.

[12] Jiawei Tao, Tao Zhang, and Yongfang Nie. "Attitude Maneuvering and Vibration Reducing Control of Flexible Spacecraft Subject to Actuator Saturation and Misalignment". In: *Shock and Vibration* 2018 (Sept. 2018), pp. 1–16. DOI: 10.1155/2018/3129834.

[13] Caleb Henry. *Eutelsat weighs adding more Quantum satellites to fleet*. https://spacenews.com/eutelsat-adding-two-more-quantum-satellites-to-fleet/. Space News. 2017.

[14] Stefano Di Gennaro. "Output stabilization of flexible spacecraft with active vibration suppression". In: *Aerospace and Electronic Systems, IEEE Transactions on* 39 (Aug. 2003), pp. 747 –759. DOI: 10.1109/TAES.2003.1238733.

[15] PETER W. LIKINS and GERALD E. FLEISCHER. "Results of flexible spacecraft attitude control studies utilizing hybrid coordinates". In: *Journal of Spacecraft and Rockets* 8.3 (1971), pp. 264–273. DOI: 10.2514/3.30258. eprint: https://doi.org/10.2514/3.30258. URL: https://doi.org/10.2514/3.30258.

[16] Shahram Shahriari, Shahram Azadi, and Majid M. Moghaddam. "An accurate and simple model for flexible satellites for three-dimensional studies". In: *Journal of Mechanical Science and Technology* 24 (June 2010). DOI: 10.1007/s12206-010-0329-0.

[17] Ohseop Song. *Modal Analysis of A Cantilever Plate*. 1986.

[18] MSC Nastran. *Service pack 1, reference guide*. Hexagon, MSC Software. 2020. URL: https://help.hexagonmi.com/bundle/MSC_Nastran_2020_Reference_Guide/resource/MSC_Nastran_2020_Reference_Guide.pdf.

[19] Manuel Beschi et al. "Using of the Robotic Operating System for PID control education". In: *IFAC-PapersOnLine* 48.29 (2015). IFAC Workshop on Internet Based Control Education IBCE15, pp. 87–92. ISSN: 2405-8963. DOI: https://doi.org/10.1016/j.ifacol.2015.11.218. URL: https://www.sciencedirect.com/science/article/pii/S2405896315024763.

[20] Mark Haidekker. "The PID Controller". In: Dec. 2013, pp. 193–208. ISBN: 9780124058750. DOI: 10.1016/B978-0-12-405875-0.00013-9.

[21] E. Capello and F. Dabbene. *Lesson 2: Control specifications and PID control*. Dispense del corso di Dinamica e Controllo di Veicoli Spaziali. Politecnico di Torino, 2019/20.

[22] *Reaction wheel 400 nNms RW-0.4 Data Sheet*. https://www.rocketlabusa.com/space-systems/satellite-components/reaction-wheels/. Rocket Lab.

[23] Hexagon. *Adams 2021.1*. MSC Adams help guide. 2021. URL: file:///C:/ADAMS/help/master.htm#page/adams_view/learn_basics_setup.01.1.html.

[24] Mohammed Chessab Mahdi, Mohammed Al-Bermani, and Mohammed Al-Bermani. "LQR Controller for Kufasat". In: *JOURNAL OF KUFA – PHYSICS* 6 (Jan. 2014), pp. 13–20.

[25] James Onojo. “Design of linear quadratic regulator for the three-axis attitude control system stabilization of microsatellites”. In: (Sept. 2018).